BMC Chemistry

RESEARCH

Open Access

Chalcone/1,3,4-Oxadiazole/Benzimidazole hybrids as novel anti-proliferative agents inducing apoptosis and inhibiting EGFR & BRAFV^{600E}

Fatma Fouad Hagar[1], Samar H. Abbas[1], Hesham A. M. Gomaa[2], Bahaa G. M. Youssif[3], Ahmed M. Sayed[4], Dalia Abdelhamid[1*] and Mohamed Abdel-Aziz[1]

Abstract

Introduction One of the most robust global challenges and difficulties in the 21st century is cancer. Treating cancer is a goal which continues to motivate researchers to innovate in design and development of new treatments to help battle the disease.

Objectives Our objective was developing new antiapoptotic hybrids based on biologically active heterocyclic motifs "benzimidazole–oxadiazole-chalcone hybrids" that had shown promising ability to inhibit EGFR and induce apoptosis. We expected these scaffolds to display anticancer activity via inhibition of BRAF, EGFR, and Bcl-2 and induction of apoptosis through activation of caspases.

Methods The new hybrids **7a-x** were evaluated for their anti-proliferative, EGFR & BRAF^{V600E} inhibitory, and apoptosis induction activities were detected. Docking study & dynamic stimulation into EGFR and BRAF^{V600E} were studied.

Results All hybrids exhibited remarkable cell growth inhibition on the four tested cell lines with IC_{50} ranging from 0.95 µM to 12.50 µM. which was comparable to Doxorubicin. Compounds **7k-m** had the most potent EGFR inhibitory activity. While, compounds **7e, 7g, 7k** and **7l** showed good inhibitory activities against BRAF^{V600E}. Furthermore, Compounds **7k, 7l,** and **7m** increased Caspases 3,8 & 9, Cytochrome C and Bax levels and decreased Bcl-2 protein levels. Compounds **7k-m** received the best binding scores and showed binding modes that were almost identical to each other and comparable with that of the co-crystalized Erlotinib in EGFR and BRAF active sites.

Conclusion Compounds **7k-m** could be used as potential apoptotic anti-proliferative agents upon further optimization.

Keywords Benzimidazole, Oxadiazole, Chalcone, Apoptosis, Anticancer Agents, EGFR, BRAF^{V600E}

*Correspondence:
Dalia Abdelhamid
dalia_abdelhameed@mu.edu.eg
[1]Medicinal Chemistry Department, Faculty of Pharmacy, Minia University, Minia 61519, Egypt
[2]Pharmacology Department, College of Pharmacy, Jouf University, Sakaka 72314, Saudi Arabia
[3]Pharmaceutical Organic Chemistry Department, Faculty of Pharmacy, Assiut University, Assiut 71526, Egypt
[4]Pharmacognosy Department, Faculty of Pharmacy, Nahda University, Beni-Suef 62513, Egypt

Introduction

Treating cancer is a goal which continues to motivate researchers to innovate in design and development of new treatments to help battle the disease. Despite these efforts to combat cancer it is spreading quickly to all age groups and it is the second leading cause of death [1]. The global burden of cancer is estimated to climb to 28.4 million in 2040, representing a 47% increase over 2020 [2]. Lung, liver, stomach, breast, and colon cancer were the top five causes of cancer-related mortality worldwide [3]. Lung and breast cancers alone represent nearly one-fourth of all newly diagnosed cancer patients in 2020 [4 with lung cancer attributing to 18% of cancer mortality and breast cancer as the main cause of cancer mortality among women [5].

Apoptosis is an intriguing target for development of innovative cancer therapeutics. Normally, the apoptotic pathway becomes activated by DNA damage or uncontrolled proliferation [6]. There are two pathways that activate apoptosis: the intrinsic and extrinsic pathways which correlate with intracellular and extracellular signals [7]. The intrinsic pathway is activated in response to DNA damage and cytokine deprivation, whereas the extrinsic pathway is triggered by the immune system. The two pathways converge at the executioner caspases [3, 6, 7] which are a class of cysteine proteases that cleave target proteins required for normal cell function [8]. Activation of caspases results in plasma membrane changes and shrinking of apoptotic cells that eventually lead to cell death [9]. The intrinsic pathway is regulated by B-cell lymphoma-2 (Bcl-2) protein family which include pro-apoptotic effector proteins, proapoptotic BH3-only proteins, and antiapoptotic Bcl-2 proteins. Bcl-2 proteins inhibit apoptosis through inhibition of the proapoptotic Bcl-2 proteins, Bcl-2-associated X protein (BAX) and Bcl-2 homologous antagonist killer (BAK) [10]. BH3-only proteins inhibit the antiapoptotic Bcl-2 proteins [11].

Apoptosis evasion is essential for survival of cancer cells and leads to increasing invasiveness, stimulating angiogenesis, deregulation of cell proliferation, and interference with differentiation. Usually, the predominant methods of apoptosis evasion include inhibition of intrinsic pathway and caspase function, overexpression of antiapoptotic Bcl-2 proteins, and loss of BAX and/or BAK [12]. This results in resistance to any intrinsic apoptotic stimuli which includes some anticancer drugs [13].

Epidermal growth factor receptor (EGFR) and B-RAF play a role in regulating the mitogen-activated protein (MAP) kinase pathway which affects cell division, differentiation, and could lead to abnormal cell proliferation [14]. Signaling pathways of EGFR control angiogenesis, activation, and regulation of cellular proliferation. Overexpression of the EGFR gene and mutations of the EGFR tyrosine kinase domain were reported in the development and progression of different carcinomas including lung, colorectal, breast, brain, and pancreas [15]. Therefore these genetic alterations showed high probability to respond to EGFR small molecule tyrosine kinase inhibitors (TKI). Additionally, a recent study has shown that suppression of EGFR signaling was correlated to induction of intrinsic apoptosis in sensitive non-small cell lung cancer (NSCLC) EGFR-mutant cell lines [16]. However, EGFR inhibitors have exhibited limited efficacies and have been challenged by innate and acquired resistance in the clinic [17].

Erlotinib, is one of the most popular EGFR inhibitors which is currently marketed to treat many types of cancer with EGFR gene mutations (including non-small lung and pancreatic cancer) [18]. Its anticancer activity drives from suppressing intracellular phosphorylation of TK at the ATP binding site of the receptor, inhibiting JAK2V617F; a mutant version of JAK2 and inducing apoptotic cell death pathways [19]. Despite its high potency, selectivity, and acceptable safety profile, patients rapidly develop resistance within 8–12 months from the start of treatment *via* mutation in the ATP binding pocket of the EGFR kinase domain [20].

EGFR signaling is a part of a complex network that has been the target of effective cancer therapies. However, emergence of resistance is a major hurdle to developing an effective anticancer regimen [21]. The combination of an EGFR inhibitor and a BRAF inhibitor synergizes and improves anticancer activity through induction of apoptosis, as demonstrated by the combination of dabrafenib with cetuximab in colorectal cells [22]. Therefore, combination therapy that combines an anti-EGFR, anti-BRAF, and apoptotic agent may exhibit a multi-pronged approach that can be developed into a highly attractive and specific molecular oriented remedy.

In our continued research efforts to develop antiapoptotic hybrids based on biologically active heterocyclic motifs we have discovered that benzimidazole–oxadiazole-chalcone hybrids have shown promising ability to inhibit EGFR and induce apoptosis. [23–25]. Individually each motif has been reported as an effective anticancer scaffold with mechanisms of action as either EGFR inhibitor, BRAF inhibitor, or inducer of apoptosis [24, 26, 27]. In this study we explored new chemical architectures attaching the benzimidazole directly to oxadiazole and chalcone. In these compounds variably substituted aromatic rings were attached to the 2-position of benzimidazole. We envisioned this structural modification would afford improved compounds capable of interacting with EGFR and stimulating caspase-3 to induce apoptosis.

Based on the previous silico molecular docking simulations using MOE software for the most active compounds and Erlotinib into ATP binding sites it was found that Erlotinib forms 2 H-bond interactions with Met769

and Gln767 and one cation…π interaction with Leu 820. None of the earlier benzimidazole- chalcone hybrids showed identical binding interactions as Erlotinib with the same amino acid residues. Moreover, the most potent EGFR inhibitors had one H-bonding interaction with Met769 as Erlotinib which meant this interaction was essential for activity. The new design moved the aromatic ring to a distal substitution on benzimidazole to introduce more flexibility in the structure. This modification allows the benzimidazole ring to be in closer proximity to more amino acids which are important for interaction with Erlotinib.

Herein, we report the design, synthesis and various biological evaluations of hybrid molecules formed from benzimidazole, oxadiazole, and chalcone derivatives aimed to improve anticancer activity by synergetic effect, decrease side effects, and minimize emergence of drug resistance. We expected these scaffolds to display anticancer activity *via* inhibition of BRAF, EGFR, and Bcl-2 and induction of apoptosis through activation of caspases. We present the synthetic strategy for preparing twenty-four new compounds, the results of detailed anticancer screening, and molecular docking. Lastly, mechanistic investigations of the most active compounds **7k**, **7L**, and **7m** regarding EGFR and BRAF inhibition and induction of caspases are described.

Results and discussion

Chemistry

The series of chemical reactions that were employed to prepare targeted benzimidazole-chalcone hybrids **7a-x** is illustrated in Fig. 1. First, substituted 2-phenyl-1 *H*-benzo[*d*]imidazole-5-carboxylic acids **1a-e** were synthesized through condensation of 3,4-diaminobenzoic acid with the appropriate aldehyde adduct in the presence of DMF for 3–6 h [28–29]. Fisher esterification of the resulting benzimidazole carboxylic acids **1a-e** with absolute ethanol using catalytic amount of concentrated H_2SO_4 as a dehydrating agent with heating for 20 h at reflux afforded the corresponding ethyl ester compounds **2a-e** [30]. Carbohydrazide compounds **3a-e** were prepared by heating the esters **2a-e** with hydrazine mono hydrate for 6–7 h at reflux [30]. Consequently, the carbohydrazide compounds **3a-e** were converted to 1,3,4 oxadiazole-benzimidazole derivatives **4a-e** by heating with carbon disulfide and KOH in absolute ethanol overnight [23, 29].

Chalcone intermediates **5a-e** were prepared by Claisen Schmidt condensation in the presence of KOH. A series of 2-bromo-*N*-(4-cinnamoylphenyl)acetamide derivatives [30].**6a-e** were synthesized by reaction of the appropriate chalcone with bromoacetyl bromide at 0° C in a biphasic medium (DCM/water) using K_2CO_3 as a base [30]. Finally, the alkylation reaction that affords target compounds **7a-x** was accomplished by coupling the oxadiazole and acetylated chalcone in the presence triethylamine and acetonitrile as solvent in good yields ranging from 73–89% [30]. The structure of the new compounds was confirmed *via* NMR and mass spectral analyses. ^{1} H NMR spectra of compounds showed singlet signal or two singlets due to rotamers at δ: 4.14–4.46 ppm related to (S-CH_2-CO). On other hand, in all compounds, the two protons of chalcone appear in the aromatic region as two doublet signals at δ: 7.56–7.74 ppm and δ: 7.80–8.16 ppm with coupling constant range J=15.2–15.6. Additionally, the amide proton of the linker NH appears as singlet signal at δ: 10.83–11.16 ppm and benzimidazole proton NH appears as singlet signal at δ: 13.10-13.48 ppm. ^{13} C NMR spectra of compounds showed two carbonyl groups related to C=O of chalcone and N-C=O appeared at δ: 186.96-189.12 ppm and 160.22–169.50 ppm, furthermore, SCH_2 appears at δ: 43.63–47.58 ppm.

Biological evaluation

Anti-proliferative assays

In vitro one-dose anti-proliferative screening in NCI The twenty-four synthesized compounds were submitted to the National Cancer Institute (NCI), USA. Eighteen hybrids **7a-h**, **7k-r**, **7u**, and **7v** were selected by NCI for one-dose assessment of their anti-proliferative activities at 10 μM dose by Sulforhodamine B colorimetric assay. The assessment was performed in 60 cell lines derived from nine tumor subpanels, comprising lung, leukemia, melanoma, colon, renal, CNS, prostate, breast, and ovarian cancer cell lines.

The one-dose NCI results revealed that the tested hybrids displayed remarkable anti-proliferative activities especially hybrids **7e**, **7k**, and **7m-o** (Figs. 70, 71, 72, 73, 74, 75, 76, 77, 78, 79, 80, 81, 82, 83, 84, 85, 86, 87 and 88 in supporting information). The most potent compound was hybrid **7k** which displayed moderate to high anti-proliferative activities against eighteen cell lines including lung, leukemia, melanoma, colon, renal, breast, and CNS cancer cell lines with growth percentages ranging from 13 to 67% (Fig. 2). Moreover, eight compounds **7g**, **7h**, **7k-m**, **7p**, **7q**, and **7v** exhibited strong anti-proliferative activities in LOX IMVI with growth percentages ranging from −32 to 18%. While **7e** and **7n** showed moderate activities against LOX IMVI with growth percentages 56% and 44%, respectively. In addition, **7e** and **7k** demonstrated moderate anti-proliferative activity against the CCRF-CEM cell line, with growth percent ranging from 38 to 52%. Compounds **7e**, **7g**, **7k**, and **7n** also displayed moderate anti-proliferative activities against the SR cell line with growth percentages ranging from 26 to 50%. Moreover, compounds **7c, 7e**, **7g**, **7k**, **7m**, **7p**, and **7v** exhibited notable anti-proliferative activity against the RPMI-8226 cell line with growth percentage

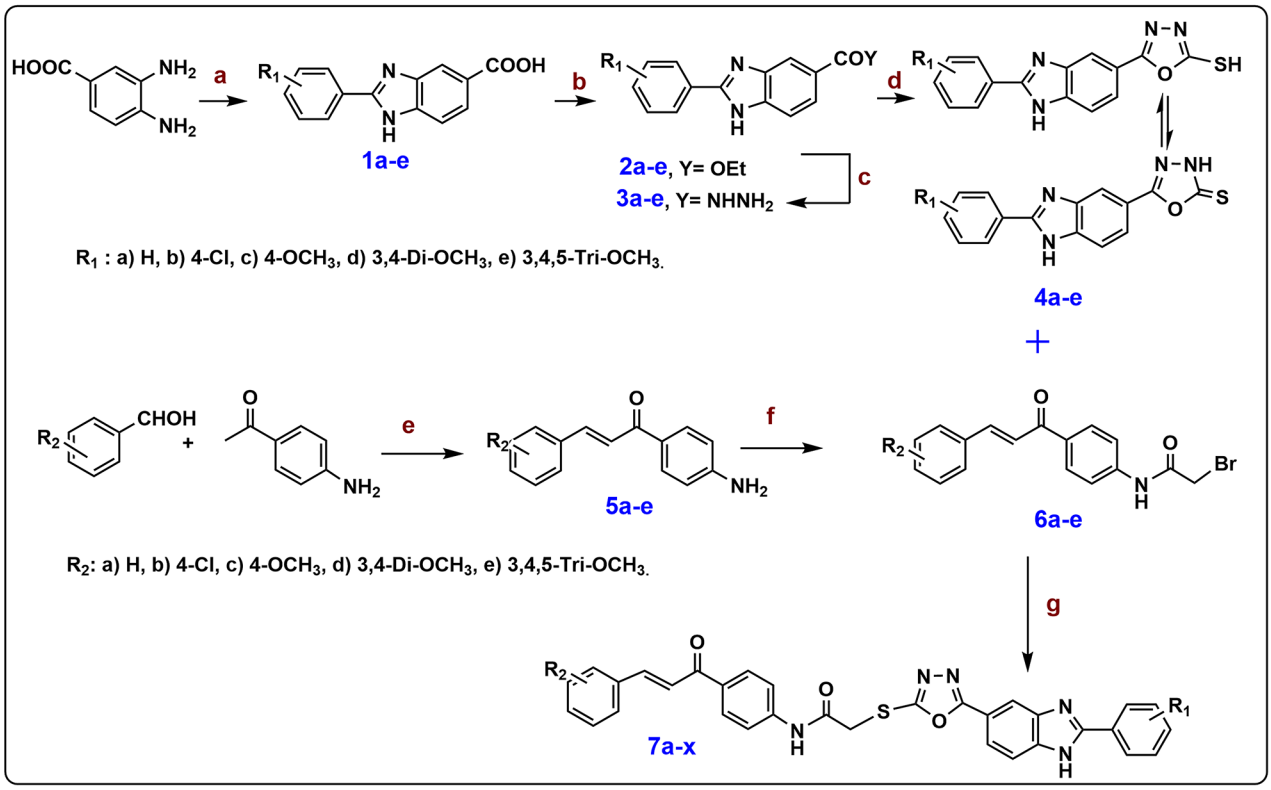

Compound	R_1	R_2	Compound	R_1	R_1
7a	H	H	**7m**	4-OCH_3	4-OCH_3
7b	H	4-Cl	**7n**	4-OCH_3	3,4-di-OCH_3
7c	H	4-OCH_3	**7o**	4-OCH_3	3,4,5-tri-OCH_3
7d	H	3,4-di-OCH_3	**7p**	3,4-di-OCH_3	H
7e	H	3,4,5-tri-OCH_3	**7q**	3,4-di-OCH_3	4-Cl
7f	4-Cl	H	**7r**	3,4-di-OCH_3	4-OCH_3
7g	4-Cl	4-Cl	**7s**	3,4-di-OCH_3	3,4-di-OCH_3
7h	4-Cl	4-OCH_3	**7t**	3,4-di-OCH_3	3,4,5-tri-OCH_3
7i	4-Cl	3,4-di-OCH_3	**7u**	3,4,5-tri-OCH_3	H
7j	4-Cl	3,4,5-tri-OCH_3	**7v**	3,4,5-tri-OCH_3	4-Cl
7k	4-OCH_3	H	**7w**	3,4,5-tri-OCH_3	4-OCH_3
7l	4-OCH_3	4-Cl	**7x**	3,4,5-tri-OCH_3	3,4-di-OCH_3

Fig. 1 Scheme for synthesis of benzimidazole/chalcone hybrids 7a-x. **Reagent and reaction conditions: (a)** The appropriate sodium hydroxy(phenyl) methanesulfonate adduct, DMF, reflux 3-6 h; **(b)** EtOH, Conc. H_2SO_4, reflux 20 h; **(c)** NH_2NH_2, EtOH, reflux 3-7 h; **(d)** 1- CS_2, KOH, EtOH, reflux 12 h.; 2- Conc HCl, (60.0-87.0%).; **(e)** KOH (60%), EtOH, stirring at 0 C for 3 h, then stirring at rt overnight; **(f)** $BrCH_2COBr$, CH_2Cl_2, K_2CO_3, H_2O, stirring overnight; **(g)** TEA, Acetonitrile, rt, 24-48 h

range 4.95–56%. Furthermore, compound **7e**, **7k**, and **7n** showed moderate anti-proliferative activities in K-562 cell line with growth percent range 58%, 55% and 47% respectively. Also, compounds **7e** and **7k**, displayed moderate anti-proliferative activities against MOLT-4 cell line (growth percent 30% and 47%, respectively). Concerning HCT-116 cell line, four compounds; **7e**, **7k**, **7n**, and **7o** exhibited moderate activity against it with growth percentages equal to 40.76%, 58.69%, 57.96%, and 50.04%, respectively. On the other hand, compounds **7e**, **7g**, **7k**, **7n**, **7o**, and **7u-v** displayed moderate activities against MCF-7 cell line with growth percentages ranging from 42.88 to 59.08%. Additionally, compound **7e** displayed higher potency against proliferation of RXF 393 cell line with growth percent equal to -6.89%. Moreover, compounds **7c** and **7k** showed significant anti-proliferative activities against T-47D cell line with growth percentages equal to 52.35% and 42.05%, respectively.

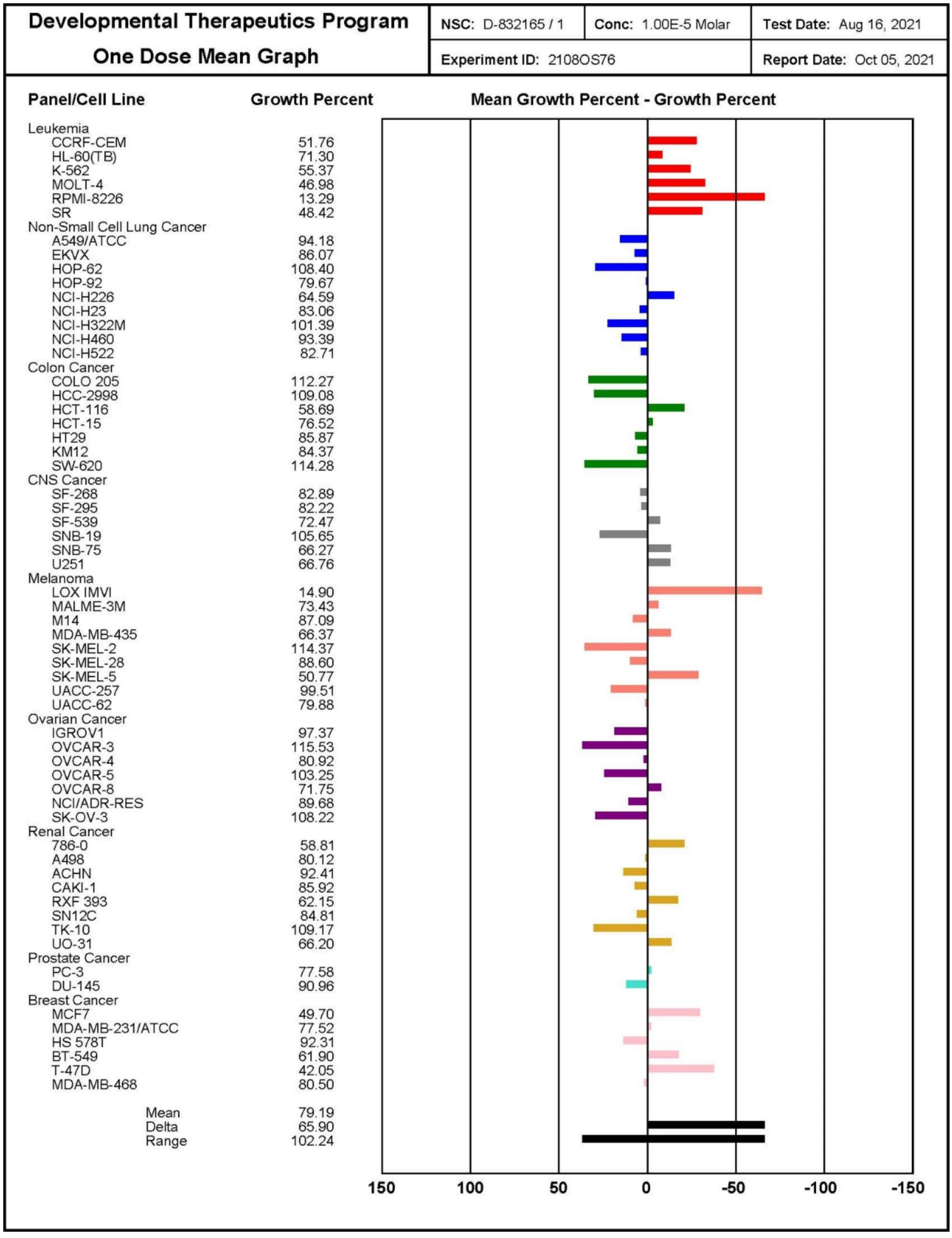

Fig. 2 One dose mean graph for compound 7k on nine different cancer cell line panels at Conc 10 μM

Table 1 IC_{50} of 7g, 7L, 7p, 7q, 7v, and Staurosporine in melanoma LOX-IMVI cell line upon 48 h incubation

Compound	7g	7l	7p	7q	7v	Staurosporine
IC_{50} ± SEM (μM)	1.05 ± 0.10	0.80 ± 0.10	1.20 ± 0.10	2.50 ± 0.20	0.90 ± 0.10	7.10 ± 0.05

Table 2 Cell viability % of MCF-10 A cells upon treatment with 50 μM of compounds 7a-x for 96 h and IC50 of compounds 7a-x & Doxorubicin in A-549, MCF-7, Panc-1 and HT-29 after 48 h incubation

Compound	Cell viability % in MCF-10 A (50 μM)	IC_{50} ± SEM (μM)			
		A-549	MCF-7	Panc-1	HT-29
7a	91	9.90 ± 1.10	9.20 ± 1.10	10.40 ± 1.30	11.15 ± 1.40
7b	88	8.20 ± 0.90	7.90 ± 0.80	8.40 ± 1.00	9.10 ± 1.10
7c	87	4.70 ± 0.50	4.15 ± 0.50	5.20 ± 0.40	5.50 ± 0.50
7d	89	9.70 ± 1.10	8.90 ± 1.10	10.30 ± 1.30	11.10 ± 1.40
7e	87	1.60 ± 0.30	1.25 ± 0.08	1.70 ± 0.30	1.95 ± 0.30
7f	87	2.15 ± 0.50	2.05 ± 0.50	2.40 ± 0.60	2.70 ± 0.50
7g	91	1.80 ± 0.60	1.45 ± 0.30	1.90 ± 0.50	2.10 ± 0.60
h	87	1.95 ± 0.60	1.75 ± 0.40	2.05 ± 0.50	2.25 ± 0.60
7i	84	9.70 ± 1.10	9.20 ± 1.00	10.15 ± 1.20	10.20 ± 1.30
7j	89	9.95 ± 1.10	9.40 ± 1.20	10.30 ± 1.20	10.70 ± 1.10
7k	91	1.20 ± 0.20	0.95 ± 0.08	1.30 ± 0.20	1.40 ± 0.20
7l	89	1.45 ± 0.30	1.10 ± 0.10	1.50 ± 0.30	1.65 ± 0.30
7m	94	1.40 ± 0.50	1.20 ± 0.08	1.50 ± 0.20	1.85 ± 0.40
7n	92	1.90 ± 0.60	1.65 ± 0.30	2.05 ± 0.50	2.20 ± 0.60
7o	89	7.60 ± 0.30	7.10 ± 0.60	8.20 ± 1.20	8.60 ± 0.40
7p	87	2.50 ± 0.50	2.10 ± 0.20	3.10 ± 0.40	3.30 ± 0.40
7q	94	3.40 ± 0.40	3.02 ± 0.30	3.80 ± 0.50	3.70 ± 0.50
7r	91	3.60 ± 0.50	3.10 ± 0.50	3.90 ± 0.50	4.20 ± 0.50
7s	87	3.80 ± 0.60	3.15 ± 0.50	4.30 ± 0.60	4.55 ± 0.60
7t	88	10.60 ± 1.10	10.10 ± 1.00	10.90 ± 1.20	10.80 ± 1.20
7u	90	2.25 ± 0.50	2.10 ± 0.08	2.40 ± 0.20	2.70 ± 0.50
7v	87	2.45 ± 0.50	2.20 ± 0.08	2.60 ± 0.20	2.90 ± 0.50
7w	91	10.90 ± 1.10	10.20 ± 1.20	11.15 ± 1.20	11.20 ± 1.30
7x	85	11.50 ± 1.20	10.800 ± 1.10	11.80 ± 1.20	12.50 ± 1.50
Doxorubicin	-	1.21 ± 0.10	0.90 ± 0.10	1.41 ± 0.10	1.01 ± 0.10

In vitro anti-proliferative assay in LOX-IMVI NCI in vitro anti-proliferative screening of compounds **7a-x** showed preferable activity against melanoma LOX-IMVI cell line over other cell lines. Specifically, five compounds; **7g**, **7l**, **7p**, **7q**, and **7v** showed remarkable anti-proliferative activities against it with growth percentages equal to -24.15%, -29.94%, -11.79%, 3.17%, and −31.58%, respectively. Consequently, the half-maximal inhibitory concentration (IC_{50}) of these compounds was determined in LOX-IMVI cell line using propidium iodide (PI)[31, 32] with Staurosporine (broad spectrum protein kinase inhibitor) as a reference. Interestingly, the five compounds displayed an IC_{50} lower than that of Staurosporine (as shown in Table 1). It is noteworthy that four of these compounds contain the *para*-chloro chalcone motif (except **7p**).

In vitro anti-proliferative assays in Panc-1, A-549, MCF-7, and HT-29 cells The propidium iodide (PI) tests[31, 32] were further used for assessment of the IC_{50} of all synthesized compounds and compared to Doxorubicin as a positive control against four cancer cell lines; pancreatic cancer cell line (Panc-1), epithelial line cancer cell (A-549), breast cancer cell line (MCF-7), and colon cancer cell line (HT-29).

As presented in Table 2, all tested hybrids exhibited remarkable cell growth inhibition on the four tested cell lines with IC_{50} ranging from 0.95 μM to 12.50 μM which was comparable to Doxorubicin (IC_{50} ranging from 0.90 μM to 1.41 μM). The most effective compound was **7k** with IC_{50} ranging from 0.95 μM to 1.40 μM and the second most active one was **7L** with IC_{50} ranging from 1.10 μM to 1.65 μM. It was observed that the highest activity was displayed by compounds; **7k**, **7L**, and **7m** in which R_1=4-OCH_3. Additionally, these hybrids showed similar effects on the Panc-1, A-549, and HT-29 cell lines with slight variation in IC_{50} values. Our structure-activity relationship (SAR) analysis revealed that the anticancer activity is reliant on pattern of substitution in both phenyl rings (Fig. 3). Anticancer activity was correlated to substitution on phenyl ring attached to position two of

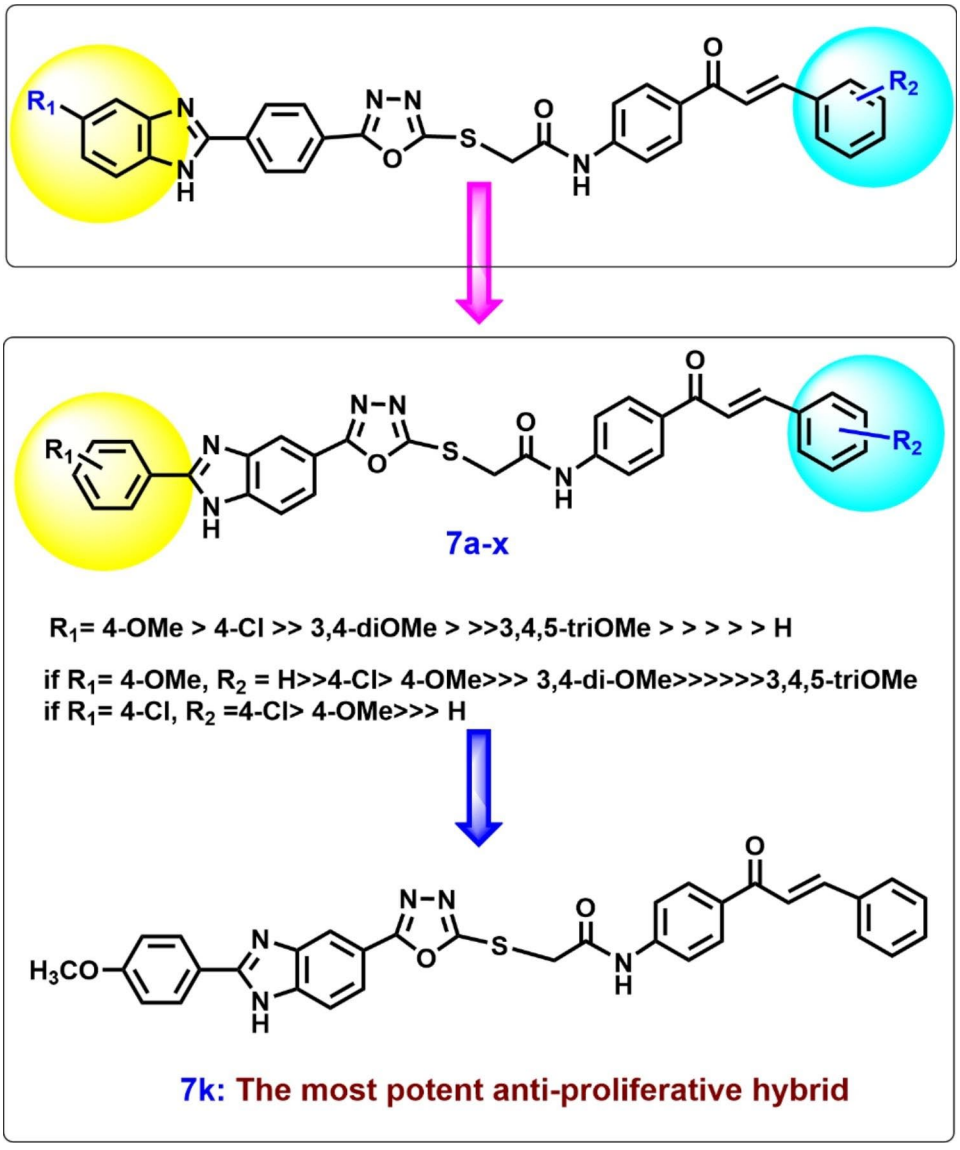

Fig. 3 The effect of compounds derivatization on anti-proliferative activity

benzimidazole ring with an effective substitution order of *p*-methoxy group>*p*-chlorine atom >>> 3,4-*di*methoxy groups. Further, it was noted that for optimal activity with p-chlorine on phenyl ring the substitution order on the chalcone phenyl ring was *p*- chlorine>*p*-methoxy >>> H.

In vitro toxicity assay in normal cells (cell viability assay) To check the safety of prepared compounds and evaluate their selectivity towards tumor cells over normal ones, the toxicity of compounds **7a-x** were evaluated by 3-(4,5-Dimethylthiazole-2-yl)-2,5-diphenyltetrazol (MTT) assay on the normal human mammary epithelial cell line (MCF-10 A) [33, 34]. The human mammary epithelial cell lines were incubated for four days with a concentration of 50 µM of compounds **7a-x**. All compounds showed cell viability of more than 80% (Table 2.). The cytotoxic activity of **7k** against MCF-7 was 96-fold higher than its toxicity against MCF-10 A. Similarly compounds **7L** and **7v** were 111 and 97-fold more selective towards LOX-IMVI cell line respectively.

EGFR inhibitory activity assay

To explore the molecular mechanism of the synthesized hybrids, an assessment of the EGFR inhibitory ability of the most potent ten compounds was performed using the EGFR-TK assay [35, 36]. The most active compounds; **7e**, **7g**, **7h**, **7k-n**, **7p**, **7q**, and **7v** were selected to determine their enzymatic inhibitory activity and compared to Erlotinib and the findings are included in Table 3. The results showed that the tested compounds inhibited EGFR with IC_{50} values ranging from 0.55 µM to 3.90 µM. The most

Table 3 Inhibitory activities of selected compounds against EGFR and BRAFV600E

Compound	EGFR Inhibition $IC_{50} \pm SEM$ (μM)	$BRAF^{V600E}$ Inhibition $IC_{50} \pm SEM$ (μM)
7e	1.15 ± 0.20	0.90 ± 0.10
7g	1.70 ± 0.20	1.00 ± 0.20
7h	2.30 ± 0.20	2.70 ± 0.30
7k	0.55 ± 0.10	1.70 ± 0.20
7L	0.80 ± 0.10	1.90 ± 0.20
7m	0.90 ± 0.10	2.20 ± 0.20
7n	1.40 ± 0.20	3.70 ± 0.20
7p	3.50 ± 0.30	4.20 ± 0.30
7q	3.90 ± 0.30	4.70 ± 0.30
7v	2.80 ± 0.30	3.10 ± 0.20
Erlotinib	0.08 ± 0.01	0.06 ± 0.01

effective compound **7k** (R_1=4-OCH_3, R_2=H) demonstrated the greatest inhibitory efficacy against EGFR with an IC_{50} of 0.55 μM, being approximately 7-fold less potent than Erlotinib (IC_{50}=0.08 μM). Compounds **7L** and **7m** rank second and third in activity, with IC_{50} values of 0.80 μM and 0.90 μM, respectively. The remaining compounds displayed weak inhibitory activity against EGFR, with IC_{50} values ranging from 1.15 μM to 3.90 μM. Consequently, compounds **7k**, **7L**, and **7m** were considered promising agents which could be used as potential anti-proliferative agents targeting EGFR-TK after optimization.

$BRAF^{V600E}$ inhibitory activity

An in vitro study was carried out to assess the anti-$BRAF^{V600E}$ activity of ten compounds namely, **7e**, **7g**, **7h**, **7k-n**, **7p**, **7q**, and **7v** and compared to Erlotinib [24, 37]. The enzyme assay revealed that all ten compounds inhibited $BRAF^{V600E}$ with IC_{50} values ranging from 0.90 μM to 4.70 μM (as shown in Table 3). Compounds **7e**, **7g**, **7k** and **7l** showed good inhibitory activities against $BRAF^{V600E}$ (IC_{50}=0.90 μM, 1.00, μM, 1.70 μM, and 1.90 μM, respectively) and they were revealed to be potent inhibitors of cancer cell proliferation as well as promising EGFR inhibitors (IC_{50}=1.15 μM, 1.70 μM, 0.55 μM and 0.80 μM respectively). These encouraging results suggest that the favourable anti-proliferative activity of these compounds is mediated through inhibition of both EGFR and $BRAF^{V600E}$.

Apoptosis induction activity

Caspases assays The effects of the most active compounds; **7k**, **7l**, and **7m** on caspases (3, 8, and 9) were evaluated and compared to Doxorubicin treated and untreated cells [38]. The results showed that the tested compounds increased the level of active caspase-3 by 7–8 folds when compared to control cells; and that compounds **7k**, **7l**, and **7m** induced remarkable overexpression of caspase-3 protein level (501.60 ± 4.00, 492.50 ± 4.00 and 473.60 ± 3.50 pg/mL, respectively) and were comparable to Doxorubicin (503.50 ± 4.50 pg/mL). Compared to the untreated cells, the most active anti-proliferative derivative **7k** showed an 8-fold increase in caspase-3 level. The effect of compounds **7k**, **7l**, and **7m** on caspases 8 and 9 were also investigated to underline the role of intrinsic and extrinsic apoptotic pathways in these compounds' anti-proliferative actions. As shown in Table 4, compound **7k** increased caspase 8 and 9 levels in comparison to untreated cells by 10 and 17 folds, respectively. Compound **7l** increased caspase 8 and 9 levels by 9 and 16 folds, respectively. These results indicated that the new hybrids were capable of activating both the intrinsic and extrinsic pathways, with a stronger impact on the intrinsic pathway because caspase 9 levels were higher.

Cytochrome C assay The amount of cytochrome C in the cell is critical for caspase activation and the beginning of the intrinsic apoptosis process [31]. The results of testing compounds **7k**, **7l**, and **7m** as Cytochrome C activators were shown in Table 4. Compounds **7k**, **7l**, and **7m** increased Cytochrome C levels by 14, 13, and 11 times, respectively, when compared to untreated control cells. These results support the assumption that Cytochrome C overexpression and the activation of intrinsic apoptotic pathway were the causes of apoptosis.

Expression levels of BAX and Bcl-2 proteins The effects of compounds **7k**, **7l**, and **7m** on BAX and Bcl-2 protein levels in the MCF-7 breast cancer cell lines were studied further using Doxorubicin as a reference for comparison [39]. The results in Table 5 showed that as compared to

Table 4 Effects of compound 7k, 7l, and 7m on caspases activity and amount of Cytochrome C in MCF-7 breast cancer cells

Compound	Caspase-3		Caspase-8		Caspase-9		Cytochrome C	
	Conc (pg/mL)	Fold change	Conc (ng/mL)	Fold change	Conc (ng/mL)	Fold change	Conc (ng/mL)	Fold change
7k	501.600 ± 4.00	7.60	1.680	9.90	15.900	17.00	0.660	14.00
7l	492.500 ± 4.00	7.50	1.570	9.30	15.100	16.00	0.595	13.00
7m	473.600 ± 3.50	7.20	1.350	7.90	13.900	15.00	0.515	11.00
Doxorubicin	503.200 ± 4.20	7.65	1.750	10.00	16.200	17.40	0.604	13.10
Control	65.600	1.00	0.170	1.00	0.930	1.00	0.046	1.00

Table 5 Effects of compound 7k-m on the protein expression levels of BAX and Bcl-2

Compound	BAX		Bcl-2	
	Conc (pg/mL)	Fold change	Conc (ng/mL)	Fold reduction
7k	279.500	33.0	0.940	5.4
7l	271.600	32.0	0.975	5.2
7m	268.200	31.5	1.050	4.9
Doxorubicin	276.500	32.5	0.985	5.1
Control	8.500	1.0	5.080	1.0

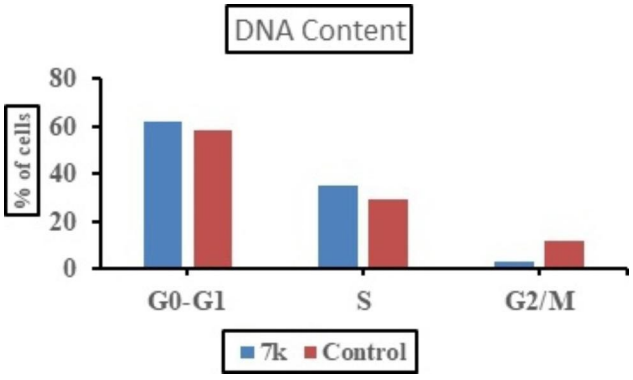

Fig. 4 Results of cell cycle analysis in untreated MCF-7 cells (Control) and MCF-7 cells treated with IC_{50} (0.95 µM) of hybrid 7k for 24 h

Doxorubicin, the compounds **7k**, **7l**, and **7m** caused a significant increase in BAX levels. Compound **7k** induction of BAX level (279.50 pg/mL) was similar to Doxorubicin (276 pg/mL) with a 33-fold increase over control untreated cancer cell, followed by compound **7l** (271 pg/mL and 32-fold rise). Finally, compound **7k** reduced anti-apoptotic Bcl-2 protein levels in MCF-7 cells to 0.94 ng/mL, followed by compound **7l** (0.97 ng/mL) in comparison to Doxorubicin (0.98 ng/mL).

Cell cycle analysis and apoptosis detection

Cell cycle analysis Compound **7k** was applied to MCF-7 cancer cell line with IC_{50} concentration (0.95 µM) to assess its effect on cell cycle progression and apoptosis induction. Data obtained from cell cycle analysis (Fig. 4) revealed that **7k** significantly increased the percentage of accumulation of MCF-7 cells in G0-G1 and **S** phase 61.95% and 34.86% respectively as compared to 58.27% and 29.51% in untreated cells. On other hand, incubation with **7k** decreased percentage accumulation in the G2/M phase to 3.19% versus 12.22% in control. From the previous results, it was concluded that compound **7k** might arrest cells at G1/S and prevent it from entering G2/M phase as indicated by decreased percentage of accumulation of cells in G2/M phase compared to control.

Apoptosis detection To further study the root for cytotoxic activity of compound **7k**, Annexin V-FITC/PI assay

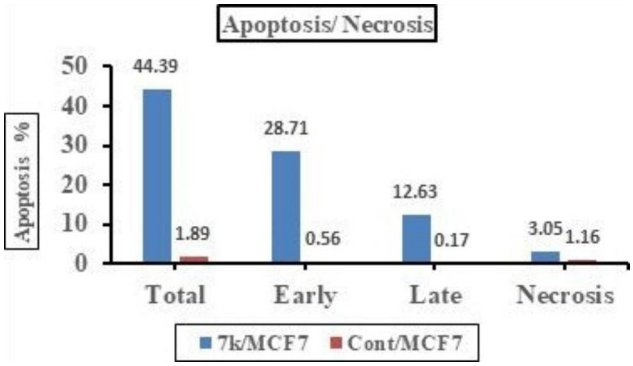

Fig. 5 Apoptosis and necrosis percentage in MCF-7 cells after incubation with DMSO (control) and with IC_{50} of compound 7k (0.95 µM) for 24 h

method[40, 41] was used to investigate its capability to induce apoptosis. In this assay MCF-7 cell line was treated with IC_{50} concentration (0.95 µM) of **7k** and stained with Annexin V/PI then incubated for 24 h. Results showed that compound **7k** increased the level of both early and late apoptosis to 28.71% and 12.63% respectively whereas necrosis level was only 3.05% (Figs. 5 and 6). These cumulative results further indicate that compound **7k** showed potent anti-proliferative activity by induction of apoptosis.

Docking study into EGFR and $BRAF^{V600E}$

The structures of the most bioactive derivatives (i.e., **7e**, **7g**, **7h**, **7k-n**, **7p**, **7q**, and **7v**) were docked inside the active sites of EGFR and BRAF to investigate their binding interactions with these proteins (Figs. 7 and 8). The resulting docking scores of these derivatives were convergent (i.e., docking scores ranged from −8.4 to -10.7 kcal/mol, Table 6) and comparable with that of the co-crystalized ligands Erlotinib and vemurafenib, respectively.

With regards to EGFR, compounds **7k**, **7l**, and **7m** received the best binding scores (-10.6, -10.7, and −10.4, respectively). Additionally, they showed binding modes that were almost identical to each other (RMSD = 0.79 Å) and comparable with that of the co-crystalized Erlotinib (docking score = -9.7 kcal/mol).

As shown in Fig. 7, each structure was able to form 2 H-bonds with MET-769 and ASP-831 amino acid residues, while the co-crystalized Erlotinib formed a single H-bond with MET-769. Additionally, the three structures (i.e., **7k**, **7l**, & **7m**) showed the same hydrophobic interactions with PHE-699, VAL-702, LYS-721, LEU-820, and LEU-834 which also interact with Erlotinib.

Similarly, **7k, 7l,** and **7m** were also the best-scoring compounds upon docking inside BRAF's active site (docking scores = -9.8, -9.9, and −9.9 kcal/mol, respectively). Moreover, they showed identical binding modes (RMSD = 0.87 Å) comparable with that of the co-crystalized inhibitors Vemurafenib and Erlotinib (docking scores = -9.6 and −9.5 kcal/mol, respectively) (Fig. 8).

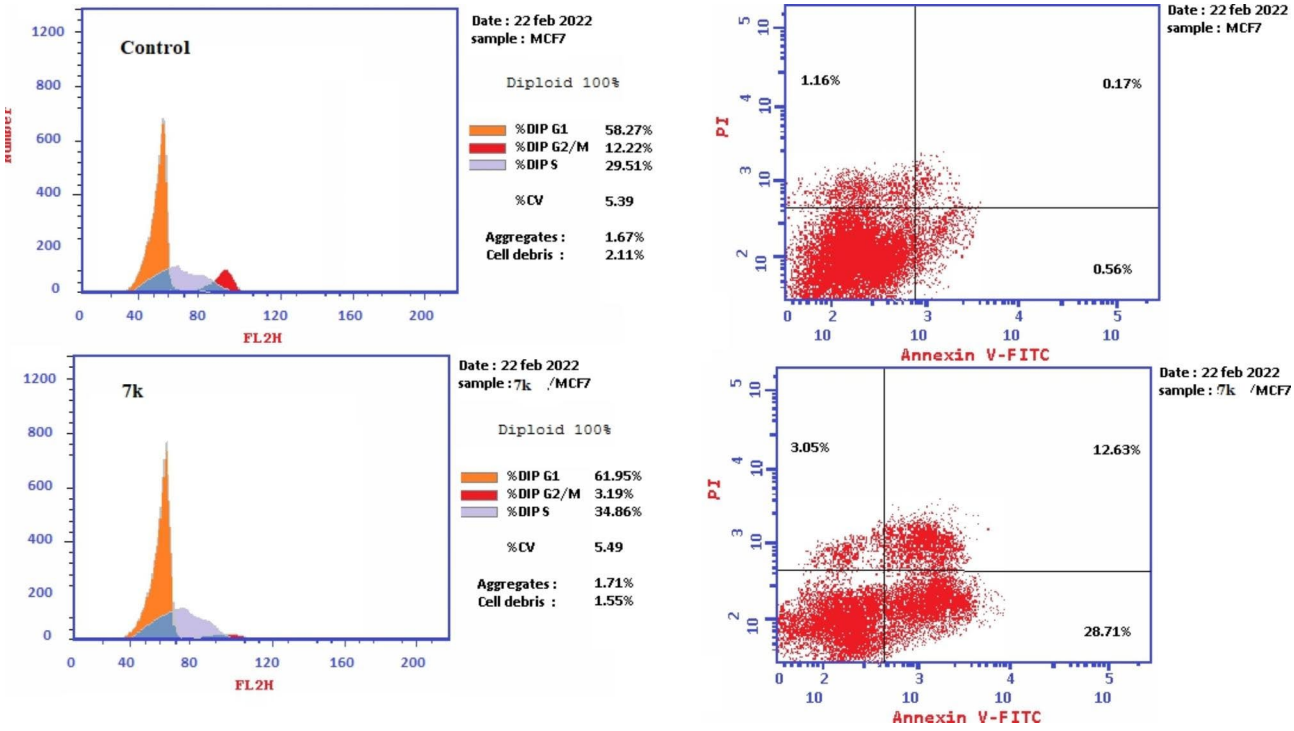

Fig. 6 Cell cycle and apoptosis induction analysis of MCF-7 cells after incubation with IC_{50} of compound 7k (0.95 µM) for 24 h using Annexin V/PI compared to control untreated MCF-7

The structures of **7k, 7l,** and **7m** were able to establish the same hydrophilic interactions (i.e. H-bonds) with THR-81, CYS-84, HIS-91, except for compound **7m** which formed additional H-bond through its additional methoxy group with SER-87 (Fig. 8A). Furthermore, the three structures also shared hydrophobic interactions with ILE-15, VAL-23, and LEU-66. Vemurafenib (the co-crystalized inhibitor) established a slightly different binding mode, where it formed 2 H-bonds with GLN-82 and CYS-84, and four hydrophobic interactions with ILE-15, VAL-23 (similarly to compounds 7k-m), LYS-35, and PHE-48 (Fig. 8B).

To further validate the docking results, the best docking poses for **7k**, **7l**, and **7m** inside the kinase domains of both EGFR and BRAF were subjected to 100 ns-long MD simulations. As shown in Fig. 9, the structures of the three compounds (i.e., 7k, 7L, and 7m) exhibited significant stability inside the active sites of both enzymes with low deviations from their initial state (i.e., docked poses) (Average RMSDs ranged from 1.9 Å to 2.2 Å). Accordingly, the calculated absolute binding free energy (ΔG_{Bind}) for each compound using the MM-PBSA method were convergent and comparable with the co-crystalized inhibitors (Erlotinib and Vemurafenib, respectively) (Table 7) [42]. Judging from the previous in silico structural analysis, it can be concluded that the derivatives **7k**, **7L**, and **7m** are considered promising structure motifs acting as EGFR and BRAF dual inhibitors.

In silico prediction of physicochemical and pharmacokinetic properties

In this study, we used two web servers Swiss ADME (http://www.swissadme.ch/index.php) and PKCSM (http://biosig.unimelb.edu.au/pkcsm/) to investigate the physicochemical and pharmacokinetic features of compounds **7k**, **7l** and **7m**. Swiss ADME affords information about SILICOS-IT, MLOGP, iLOGP, XLOGP3, and WLOGP, the distinct models that predict lipophilicity. Also, Log of Consensus Po/w is calculated by taking their arithmetic mean [43]. BOILED Egg is a map of polarity expressed in TPSA, another model for predicting lipophilicity. The yolk reflects the potential for BBB permeability in the BOILED Egg plot (Fig. 10), whereas the white represents the possibility for GI absorption. Finally, a bioavailability radar map is a plot of six different physicochemical parameters: size, polarity, flexibility, solubility, saturation, and lipophilicity. The pink hexagon in the center of the figure represents the optimal range for excellent oral bioavailability (Fig. 11) [44, 45].

PKCSM affords important information about pharmacokinetic parameters of the drug such as: Caco-2 permeability, volume of distribution at steady state (VDss), Pgp I and II inhibitors, total clearance, central nervous system (CNS) permeability, AMES toxicity, renal organic cation transporter 2 (OCT2) substrate, maximum recommended tolerated dose (MRTD) human, oral rat acute toxicity (LD_{50}) and chronic toxicity-lowest observed

Table 6 Results of the docking compounds 7e, 7g, 7h, 7k-n, 7p, 7q, and 7v into the active sites of EGFR (PDB ID: 1M17) and BRAFV600E (PDB ID: 3OG7) in comparison with their co-crystallized ligands

Compound	Docking score EGFR	Docking score $BRAF^{V600E}$	Interactions			
			H-bonding		Hydrophobic	
			EGFR	BRAF	EGFR	BRAF
7e	-8.4	-8.5	-	SER-87, HIS-91	PHE-699, VAL-702	VAL-23, LEU-66
7g	-9.2	-9.4	-	SER-87, HIS-91	PHE-699, LEU-834, LEU-820,	ILE-15, VAL-23
7h	-9.2	-9.9	-	CYS-84, SER-87, HIS-91	VAL-702, LEU-834	ILE-15, VAL-23, LEU-66
7k	-10.6	-9.8	MET-769, ASP-831	THR-81, CYS-84, SER-87, HIS-91	PHE-699, VAL-702, LEU-820, LEU-834	ILE-15, VAL-23, LEU-66
7l	-10.7	-9.9	MET-769, ASP-831	THR-81, CYS-84, HIS-91	PHE-699, VAL-702, LEU-820, LEU-834	ILE-15, VAL-23, LEU-66
7m	-10.4	-9.9	MET-769, ASP-831	THR-81, CYS-84,	PHE-699, VAL-702, LEU-820, LEU-834	ILE-15, VAL-23, LEU-66
7n	-10.1	-9.5	MET-769	THR-81, CYS-84	PHE-699, LEU-820, LEU-834	ILE-15, VAL-23, LEU-66
7p	-9.1	-9.0	-	THR-81	PHE-699, VAL-702, LEU-820	ILE-15, VAL-23
7q	-8.8	-9.1	MET-769	CYS-84	PHE-699, VAL-702, LEU-820	VAL-23, LEU-66
7v	-9.3	-9.1	ASP-831	THR-81, CYS-84	PHE-699, LEU-820, LEU-834	VAL-23, LEU-66
Erlotinib	-9.7	-9.5	MET-769	-	LEU-694, VAL-702 LEU-820	-
Vemurafenib	-	-9.6	-	GLN-82, CYS-84	-	ILE-15, VAL-23, LYS-35, PHE-48

adverse effect (LOAEL), skin sensitization, hepatotoxicity, Tetrahymena pyriformis toxicity, and LC_{50} by fathead minnow toxicity [46].

SwissADME results of compounds **7k**, **7l**, **7m**, and Erlotinib are presented in Table 8. These results indicated that compounds **7k** and **7m** obeyed Lipinski rule with one violation (M.wt > 500) while **7l** did not; with two violations: M,wt > 500 and MLOGP of 4.17 (> 4.15). Compound **7k** calculated octanol/water partition coefficient (log P) is 3.28 which is equal to Erlotinib while the log P values for **7l** and **7m** were 5.87 and 5.41, respectively. The three compounds showed low molecular flexibility (rotatable bond (RB) > 10) which may indicate poor absorption of the compounds.

All three compounds showed promising cell permeability through diverse biological membrane as topological polar surface area (TPSA) results ranged from 148.30 to 157.53 while Erlotinib was 74.73.

PKCSM results were slightly different from SwissADME results. The difference in prediction outcomes between web servers are most likely due to changes in the modules and algorithms utilized on each web server. As a result, it is critical to receive ADMET characteristics from many web servers rather than just one [47].

The results shown in Table 9, revealed that the compounds **7k**, **7l**, and **7m** displayed good values for oral absorption. Erlotinib was predicted to have a cellular permeability of 97.99% while compounds **7k**, **7l**, and **7m** values ranged from 93.26 to 98.11%. The three compounds showed higher water solubility equal to -2.89 log mol/L than Erlotinib −5.11 log mol/L. and displayed good skin permeability but low permeability in Caco2 (human colon adenocarcinoma). It was also predicted that **7k**, **7l**, and **7m** may be a substrate of the ATP-binding cassette transporter P-glycoprotein, which was found to have an inhibitory effect in epithelial cells.

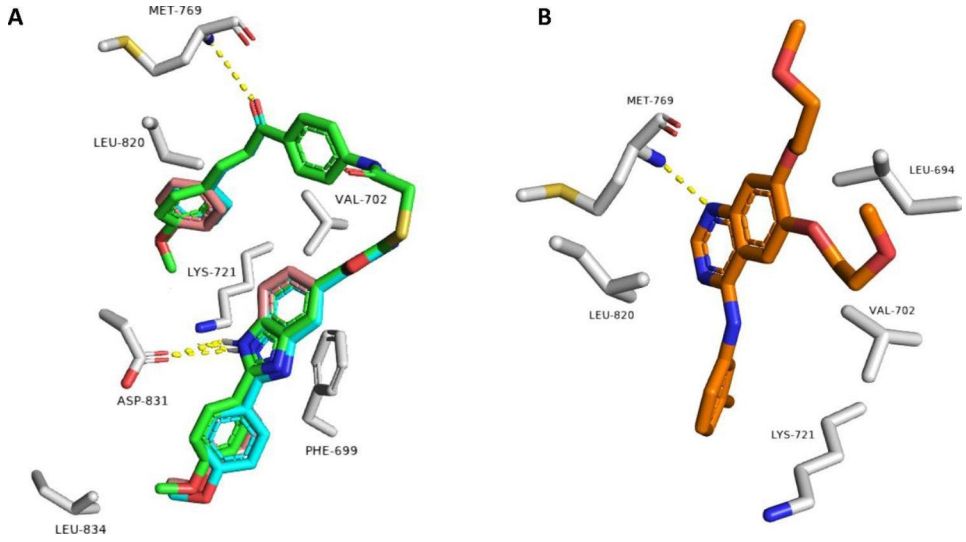

Fig. 7 A: Binding modes of compounds 7k, 7l, 7m (green, cyan, and brick red structures, respectively) inside the binding site of kinase domain of human EGFR (PDB ID: 1M17) B: Kinase domain of EGFR with the co-crystalized Erlotinib (orange-colored structure)

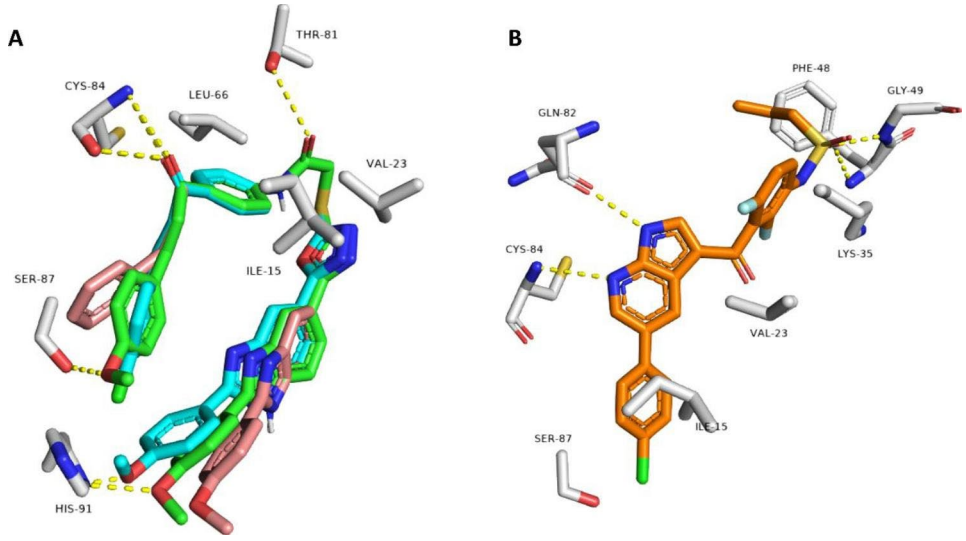

Fig. 8 A: Binding modes of compounds 7k, 7l, 7m (green, cyan, and brick red structures, respectively) inside the binding site of kinase domain of human BRAF (PDB ID: 3OG7) B: Kinase domain of EGFR with the co-crystalized Erlotinib/Vemurafenib (orange-colored structure)

Concerning distribution, the compounds showed low volume of distribution at a steady state at a value of -0.011, -0.009 and-0.038 log L/kg which was comparable to Erlotinib value of 0.167 log L/kg. Distribution parameter revealed that the compounds were poorly distributed to blood brain barrier and displayed safety in CNS. It was predicted that the three compounds have no or little drug-drug interactions as they were shown to be CYP3A4 but not CYP2D6 substrates, and CYP2C19, CYP2C9, and CYP3A4 but not CYP2D6 inhibitors.

According to excretion parameters all compounds showed better results for total clearance from liver and kidney with values of 0.678, 0.669 and 0.703 log ml/min/kg compared to Erlotinib with 0.572 log ml/min/kg value.

Furthermore, the software predicted toxicity profiles including mutagenicity and cardiotoxicity. The three compounds and Erlotinib showed similar safety profile and acceptable level profile hERG I (human ether-a-go-go-related gene I) but displayed hepatotoxicity. Based on the in-silico ADME/Tox prediction, we may infer that compounds **7k, 7l,** and **7m** may possess an acceptable pharmacokinetic and safety profile, validating its promise as an oral therapy for cancer. Complete ADMET results of testing with PKCSM are presented in Table 9.

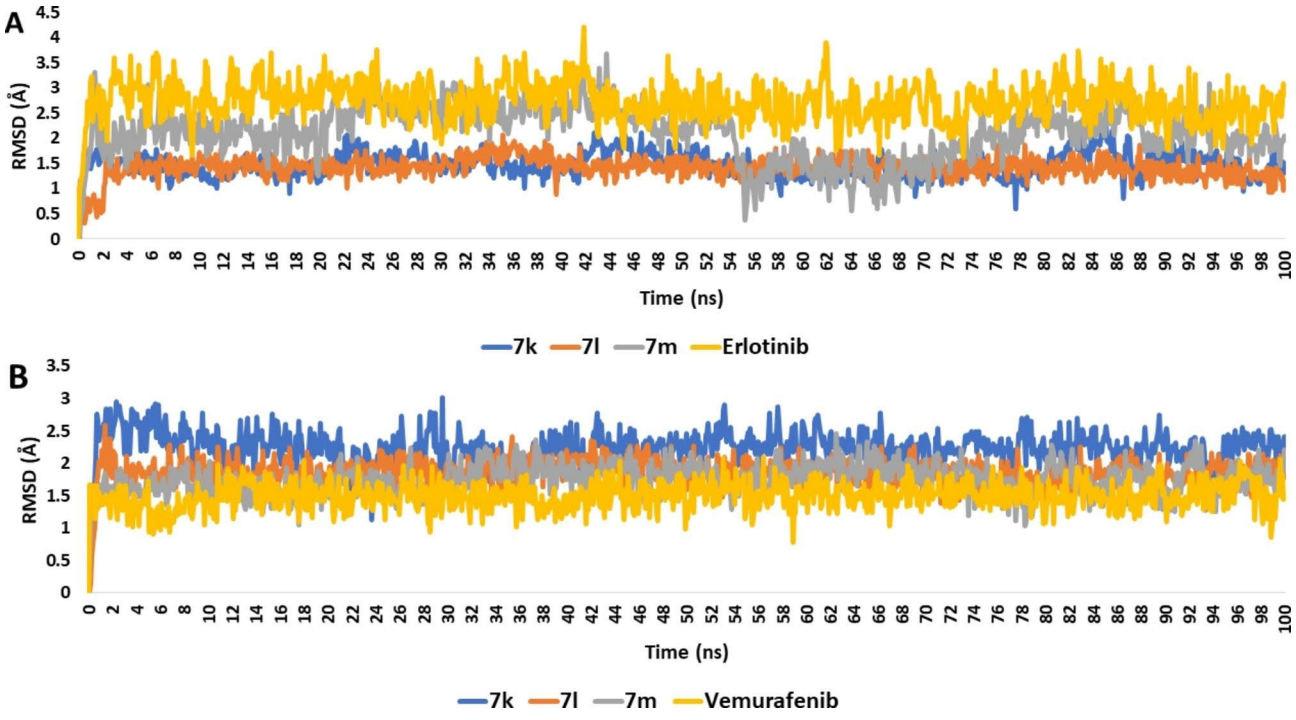

Fig. 9 RMSDs of 7k, 7l, and 7m inside the kinase domains of both EGFR and BRAF (A and B, respectively) in comparison with the previously reported co-crystalized inhibitors (i.e., Erlotinib and Vemurafenib, respectively) over the course of 100 ns-long MD simulations

Table 7 The calculated ΔG_{Bind} (in kcal/mol) of 7k, 7l, and 7m inside the kinase domains of both EGFR and BRAF (A and B, respectively) in comparison with the previously reported co-crystalized inhibitors (i.e., Erlotinib and Vemurafenib, respectively)

Energy Component	7k		7l		7m		Erlotinib	Vemurafenib
	EGFR	BRAF	EGFR	BRAF	EGFR	BRAF	EGFR	BRAF
ΔG gas	-49.3409	-53.6574	-54.9876	-53.6723	-41.8203	-49.5564	-48.1047	-48.4837
ΔG solv	14.8213	16.4637	16.7483	17.3443	11.2943	14.4463	13.6452	16.3827
ΔG TOTAL	-34.5196	-38.2393	-38.2393	-36.328	-30.526	-35.1101	-34.4595	-32.101

Conclusion

In this study we explored the apoptotic activity of new chemical architectures comprised of substituted benzimidazole moiety directly linked to an oxadiazole ring which is tethered to a chalcone derivative. The new hybrids' NCI assay results revealed that they had remarkable anti-proliferative activities, principally hybrids **7e**, **7k**, and **7m-o**. Furthermore, in vitro anti-proliferative assays revealed promising inhibitory activity against a panel of four cancer cell lines, with IC_{50} values comparable to Doxorubicin. Compounds **7k**, **7l**, and **7m** displayed promising activity in activation of caspases, inhibiting EGFR and/or $BRAF^{V600E}$, induction of BAX and inhibition of Bcl-2 proteins expression. Further docking, MD simulations, and ΔG_{Bind} experiments were conducted to study the binding modes and stability of **7k**, **7l**, and **7m** inside the kinase domains of both EGFR and BRAF. These results indicated that these compounds could be used as potential apoptotic anti-proliferative agents upon further optimization. ADMET properties of compounds **7k**, **7l**, and **7m** were predicted successfully by two web servers Swiss ADME and PKCSM. The results revealed that the compounds had an ADMET profile that is comparatively similar to Erlotinib.

Experimental section

Chemistry

General Details: See Appendix A.

General procedure for synthesis of 2-{5-[2-aryl-1 H-benzo[d] imidazol-5-yl]-1,3,4-oxadiazol-2-ylthio}-N-{4-[(E)-3-arylacryloyl]phenyl}acetamide 7a-x [25, 30]

TEA (0.18 mL/mol) was added as a base to an equimolar mixture of the proper 2-bromo-*N*-{4-[(*E*)-3-arylacryloyl] phenyl}acetamides **6a-e** (0.09 mmol) and the proper oxadiazoles **4a-e** (0.09 mmol) in acetonitrile. The reaction mixture was left to stir from 48 to 72 h at room temperature till the formation of the precipitate. The target hybrids were obtained in a good yield by filtration, drying, and recrystallization of the formed precipitate from acetonitrile.

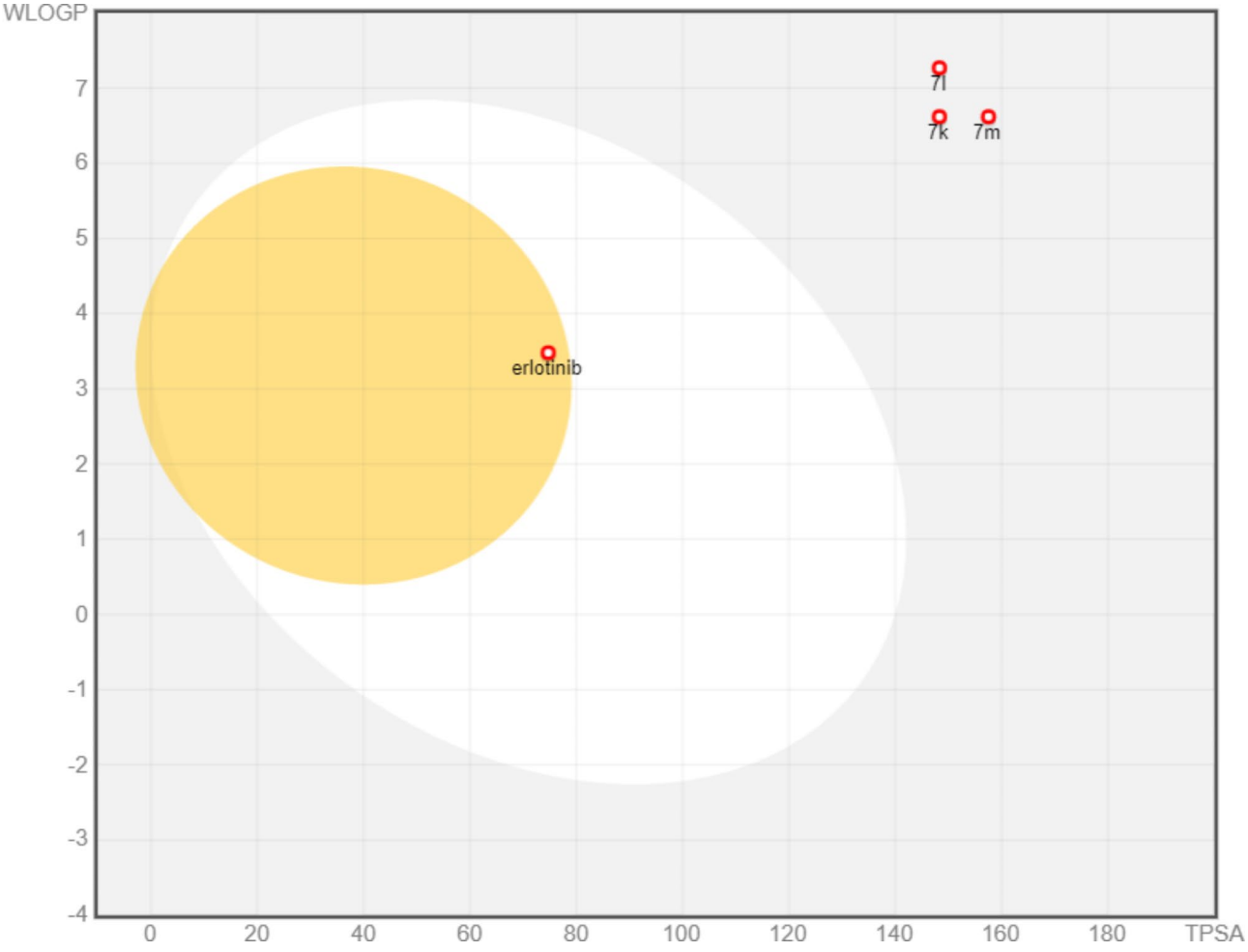

Fig. 10 Forecast Boiled-Egg plotting from Swiss ADME online website for scaffolds **7k**, **7l**, **7m**, and **Erlotinib**

2-{5-[2-Phenyl-1 *H*-benzo[*d*]imidazol-5-yl]-1,3,4-oxadiazol-2-ylthio}-*N*-{4-[(*E*)-3-phenylacryloyl] phenyl}acetamide (7a) Off-white crystal (0.21 g, 80% yield); m.p: 273–275 °C; ^{1}H NMR (500 MHz, DMSO-d_6) δ (ppm): 4.44 (2 H, s, SCH2), 7.46 (4 H, d, *J*=5.4 Hz, Ar-H), 7.52–7.60 (3 H, m, Ar-H), 7.74 (1 H, d, *J*=15.6 Hz, CH=CH), 7.82 (3 H, d, *J*=8.4 Hz, Ar-H), 7.86–7.90 (2 H, m, Ar-H), 7.95 (1 H, d, *J*=15.6 Hz, CH=CH), 8.19–8.25 (5 H, m, Ar-H), 10.86 (1 H, s, NH), 13.31 (1 H, s, NH); ^{13}C NMR (125 MHz, DMSO-d_6) δ (ppm): 46.16, 112.88, 117.44, 117.66, 118.79, 120.29, 121.43, 122.44, 126.95, 127.35, 129.51, 129.73, 129.98, 130.48, 130.86, 133.25, 134.99, 143.44, 144.07, 153.85, 153.97, 154.32, 163.15, 165.57, 166.45, 188.32; HRMS (ESI) m/z $[M+H]^+$ calcd for $C_{32}H_{23}N_5O_3S$: 558.1594, found: 558.1536.

2-{5-[2-Phenyl-1 *H*-benzo[*d*]imidazol-5-yl]-1,3,4-oxadiazol-2-ylthio}-N-{4-[(*E*)-3-(4-chlorophenyl) acryloyl]phenyl}acetamide (7b) Off-white crystal (0.19 g, 80% yield); m.p: 263–264 °C; ^{1}H NMR (500 MHz, DMSO-d_6) δ (ppm): 4.43 (2 H, s, SCH2), 7.52 (3 H, d, *J*=8.2 Hz, Ar-H), 7.53–7.60 (3 H, m, Ar-H), 7.71 (1 H, d, *J*=15.4 Hz, CH=CH), 7.81 (2 H, d, *J*=8.5 Hz, Ar-*H*), 7.92 (2 H, d, *J*=8.5 Hz, Ar-H), 7.97 (1 H, d, *J*=15.4 Hz, CH=CH), 8.16–8.24 (6 H, m, Ar-H), 10.86 (1 H, s, NH), 13.32 (1 H, s, NH); ^{13}C NMR (125 MHz, DMSO-d_6) δ (ppm): 47.58, 113.59, 117.84, 119.55, 121.26, 123.20, 127.52, 128.96, 129.47, 129.76, 130.38, 130.89, 131.48, 133.20, 134.04, 134.31, 135.14, 137.74, 138.06, 142.82, 144.02, 151.09, 153.12, 165.87, 166.46, 188.31; HRMS (ESI) m/z $[M+H]^+$ calcd for $C_{32}H_{22}ClN_5O_3S$: 592.1205, found: 592.1160.

2-{5-[2-Phenyl-1 *H*-benzo[*d*]imidazol-5-yl]-1,3,4-oxadiazol-2-ylthio}-*N*-{4-[(*E*)-3-(4-methoxyphenyl)acryloyl]phenyl}acetamide (7c) Beige crystal (0.19 g, 79% yield); m.p: 175–177 °C; ^{1}H NMR (500 MHz, DMSO-d_6) δ (ppm): 3.83 (3 H, s, OCH3), 4.26 (2 H, s, SCH2), 6.92–7.14 (3 H, m, Ar-H), 7.54–7.65 (5 H, m, 4 Ar-H+CH=CH), 7.73 (1 H, s, Ar-H), 7.80–7.90 (5 H, m, Ar-H), 8.16 (1 H, d, *J*=15.4 Hz, CH=CH), 8.23–8.39 (3 H, m, Ar-H), 10.91 (1 H, s, NH), 13.34 (1 H, s, NH); ^{13}C NMR (125 MHz,

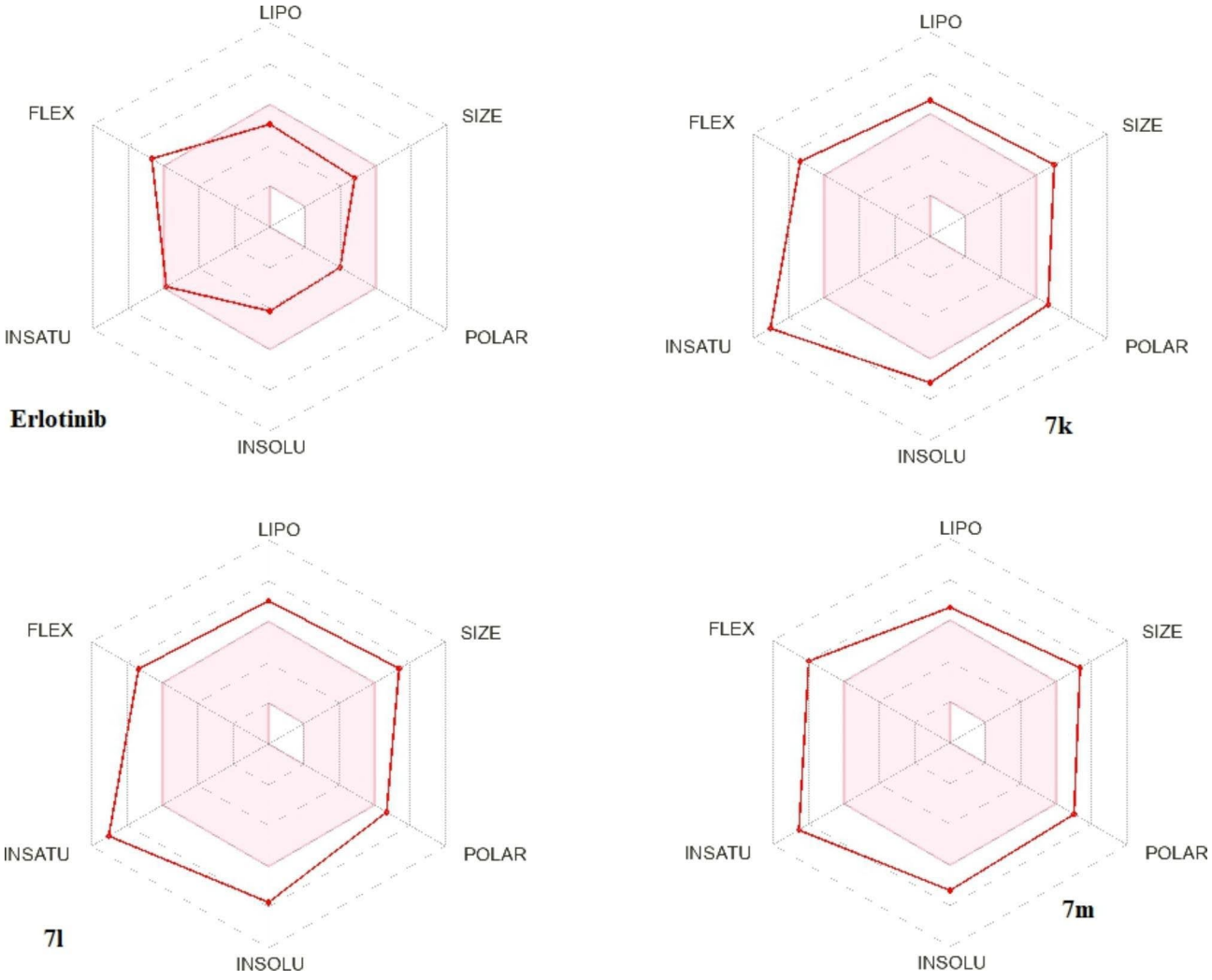

Fig. 11 Radar bioavailability diagram from Swiss ADME website for scaffolds **7k**, **7l**, **7m**, and **Erlotinib**. The pink area characterizes the optimum property values range for the oral bioavailability, and the red lines represent the forecasted characters

DMSO-d_6) δ (ppm): 43.63, 55.84, 114.86, 114.89, 114.91, 119.87, 119.88, 119.94, 127.06, 127.12, 127.24, 129.01, 129.03, 129.49, 129.51, 129.53, 129.62, 131.16, 131.38, 138.12, 139.15, 144.01, 145.35, 153.41, 161.97, 163.32, 187.81; HRMS (ESI) m/z $[M+H]^+$ calcd for $C_{33}H_{25}N_5O_4S$: 588.1700, found: 588.1620.

2-{5-[2-Phenyl-1 *H*-**benzo[***d***]imidazol-5-yl]-1,3,4-oxadiazol-2-ylthio}-***N*-**{4-[(***E***)-3-(3,4-dimethoxyphenyl) acryloyl]phenyl}acetamide (7d)** Dark brown (0.20 g, 83% yield); m.p: 156–158 °C; ^{1} H NMR (500 MHz, DMSO-d_6) δ (ppm): 3.82 (3 H, s, OCH3), 3.87 (3 H, s, OCH3), 4.45 (2 H, s, SCH2), 7.02 (1 H, d, *J*=8.4 Hz, Ar-H), 7.38 (1 H, d, *J*=8.4 Hz, Ar-H), 7.54 (1 H, s, Ar-H), 7.56–7.60 (3 H, m, 2 Ar-H+CH=CH), 7.69 (1 H, d, *J*=15.4 Hz, CH=CH), 7.76 (1 H, d, *J*=8.4 Hz, Ar-H), 7.84 (3 H, d, *J*=8.4 Hz, Ar-H), 7.86 (1 H, s, Ar-H), 7.89–7.96 (1 H, m, Ar-H), 8.20 (2 H, d, *J*=8.0 Hz, Ar-H), 8.24 (2 H, d, *J*=8.0 Hz, Ar-H), 11.01 (1 H, s, NH), ^{13} C NMR (125 MHz, DMSO-d_6) δ (ppm): 45.89, 56.06, 56.22, 111.12, 111.95, 118.87, 119.13, 119.93, 124.28, 125.29, 127.20, 127.97, 129.29, 129.49, 129.88, 129.95, 130.22, 130.77, 133.42, 134.03, 143.20, 143.45, 144.37, 149.52, 151.70, 154.21, 163.06, 166.18, 166.55, 187.79; HRMS (ESI) m/z $[M+K]^+$ calcd for $C_{34}H_{27}N_5O_5S$: 656.1364, found 656.1407.

2-{5-[2-Phenyl-1 *H*-**benzo[***d***]imidazol-5-yl]-1,3,4-oxadiazol-2-ylthio}-***N*-**{4-[(***E***)-3-(3,4,5-trimethoxyphenyl) acryloyl]phenyl}acetamide (7e)** Dark brown (0.21 g, 85% yield); m.p: 143–144 °C; ^{1} H NMR (500 MHz, DMSO-d_6) δ (ppm): 3.73 (3 H, s, OCH3), 3.88 (6 H, s, 2OCH3), 4.26 (1.20 H, s, SCH2), 4.45 (0.80 H, s, SCH2), 7.24 (2 H, s, Ar-H), 7.54 (1 H, d, *J*=7.1 Hz, Ar-H), 7.57–7.60 (4 H, m, Ar-H), 7.70–7.74 (2 H, m, 1 Ar-H+CH=CH), 7.84 (1 H, d, *J*=8.5 Hz, Ar-H), 7.94 (1 H, d, *J*=15.3 Hz, CH=CH), 8.18 (1 H, d, *J*=8.5 Hz, Ar-H), 8.23 (3 H, d, *J*=8.5 Hz, Ar-H),

Table 8 ADMET Results of the test with SwissADME for the target compounds **7k, 7l, 7m,** and Erlotinib

Compound	M.Wt	Fraction Csp3	RB	HBA	HBD	MR	TPSA	Log P	GI absorption	BBB perm.	Lip. V.	Bio. Sc.
7k	587.65	0.06	11	7	2	166.67	148.30	3.28	Low	No	Yes	0.55
7l	622.09	0.06	11	7	2	171.68	148.30	5.87	Low	No	No	0.17
7m	617.67	0.09	12	8	2	173.17	157.53	5.41	Low	No	Yes	0.55
Erlotinib	393.44	0.27	10	6	1	111.40	74.73	3.28	High	Yes	Yes	0.55

Table 9 ADMET Results of the test with PKCSM for the target compounds **7k, 7l, 7m** and **Erlotinib**

Properties	7k	7l	7m	Erlotinib
LOGP	6.9154	7.5688	6.924	3.4051
Surface area	250.582	260.885	262.060	169.532
Water Solubility	-2.894	-2.894	-2.894	-5.114
Caco2 Permeability	0.133	0.026	0.114	0.877
Intestinal absorption	96.941	98.107	93.255	97.995
Skin permeability	-2.735	-2.735	-2.735	-2.802
P-glycoprotein (Pgp) substrate	Yes	Yes	Yes	No
Pgp1 inhibitor	Yes	Yes	Yes	Yes
Pgp2 inhibitor	Yes	Yes	Yes	Yes
VDss	-0.011	-0.009	-0.038	0.167
BBB permeability	-1.353	-1.534	-1.563	-0.604
CNS Permeability	-2.881	-2.824	-3.043	-3.531
CYP2D6 substrate	No	No	No	No
CYP3A4 substrate	Yes	Yes	Yes	Yes
CYP1A2 inhibitor	Yes	Yes	Yes	No
CYP2C19 inhibitor	Yes	Yes	Yes	Yes
CYP2C9 inhibitor	Yes	Yes	Yes	Yes
CYP2D6 inhibitor	No	No	No	No
CYP3A4 inhibitor	Yes	Yes	Yes	Yes
Total clearance	0.678	0.669	0.703	0.572
Renal OCT2 substrate	Yes	Yes	No	No
AMES toxicity	Yes	Yes	Yes	No
Max tolerated dose MRTDs log	0.339	0.324	0.315	0.375
hERG I inhibitor	No	No	No	No
hERG II inhibitor	Yes	Yes	Yes	Yes
Oral Rat Acute Toxicity LD_{50}	2.479	2.479	2.479	3.155
LOAEL	2.165	2.095	1.895	1.477
Hepatotoxicity	Yes	Yes	Yes	Yes
***T. Pyriformis*toxicity**	0.285	0.285	0.285	0.356
Minnow toxicity	-1.122	-1.579	-1.875	-2.252

8.32 (1 H, d, *J*=8.5 Hz, Ar-H), 10.89 (1 H, s, NH), 13.30 (1 H, s, NH); ^{13} C NMR (125 MHz, DMSO-d_6) δ (ppm): 45.99, 56.62, 60.62, 106.92, 106.95, 107.12, 118.8, 121.49, 126.56, 127.12, 127.24, 127.26, 129.01, 129.03, 129.48, 129.72, 130.17, 130.47, 130.75, 139.20, 139.63, 140.36, 144.45, 145.40, 153.56, 162.28, 168.69, 186.96; HRMS (ESI) m/z $[M+H]^+$ calcd for $C_{35}H_{29}N_5O_6S$: 648.1911, found: 648.1963.

2-{5-[2-(4-Chlorophenyl)-1 *H*-**benzo[***d***]imidazol-5-yl]-1,3,4-oxadiazol-2-ylthio}-***N*-**{4-[(***E***)-3-phenylacryloyl]phenyl}acetamide (7f)** Beige crystal (0.21 g, 84.5% yield); m.p: 161–163 °C; ^{1} H NMR (500 MHz, DMSO-d_6) δ (ppm): 4.45 (2 H, s, SCH2), 7.40–7.50 (4 H, m, Ar-H), 7.63 (2 H, d, *J*=8.3 Hz, Ar-H), 7.73 (1 H, d, *J*=15.6 Hz, CH=CH), 7.84 (3 H, d, *J*=8.3 Hz, Ar-H), 7.88 (3 H, d, *J*=8.3 Hz, Ar-H), 7.94 (1 H, d, *J*=15.6 Hz, CH=CH), 8.19 (2 H, d, *J*=8.6 Hz, Ar-H), 8.24 (2 H, d,

J=8.6 Hz, Ar-H), 11.03 (1 H, s, NH); ^{13} C NMR (125 MHz, DMSO-d_6) δ (ppm): 45.88, 117.50, 119.03, 122.39, 128.81, 128.98, 129.10, 129.26, 129.35, 129.59, 130.36, 130.45, 130.96, 133.11, 135.20, 135.67, 136.25, 143.42, 143.65, 143.92, 149.29, 155.80, 162.98, 166.37, 166.46, 188.02; HRMS (ESI) m/z $[M+H]^+$ calcd for $C_{32}H_{22}ClN_5O_3S$: 592.1205, found: 592.1152.

2-{5-[2-(4-Chlorophenyl)-1 *H*-benzo[*d*]imidazol-5-yl]-1,3,4-oxadiazol-2-ylthio}-*N*-{4-[(*E*)-3-(4-chlorophenyl)acryloyl]phenyl}acetamide (7g) Pale brown powder (0.19 g, 79.5% yield); m.p: 215–217 °C; ^{1} H NMR (400 MHz, DMSO-d_6) δ (ppm): 4.44 (2 H, s, SCH2), 7.19–7.24 (1 H, m, Ar-H), 7.50 (2 H, d, *J*=8.1 Hz, Ar-H), 7.57–7.61 (1 H, m, Ar-H), 7.69 (1 H, d, *J*=15.5 Hz, CH=CH), 7.79 (2 H, d, *J*=8.3 Hz, Ar-H), 7.88–7.95 (3 H, m, 2 Ar-H+CH=CH), 7.97 (1 H, s, Ar-H), 8.11 (2 H, d, *J*=8.0 Hz, Ar-H), 8.18 (2 H, d, *J*=8.3 Hz, Ar-H), 8.33 (2 H, d, *J*=8.0 Hz, Ar-H), 10.89 (1 H, s, NH), 13.35 (1 H, s, NH); ^{13} C NMR (125 MHz, DMSO-d_6) δ (ppm): 46.10, 111.76, 113.41, 118.96, 119.08, 120.91, 123.15, 124.44, 127.47, 127.83, 128.75, 129.40, 130.54, 130.98, 131.37, 133.08, 134.20, 135.45, 142.47, 143.56, 145.13, 151.96, 164.14, 165.29, 166.11, 187.92; Anal. calcd. for $C_{32}H_{21}Cl_2N_5O_3S$: C 61.35, H 3.38, N 11.18, S 5.12. Found: C 61.62, H 3.52, N 11.40, S 5.29.

2-{5-[2-(4-Chlorophenyl)-1*H*-benzo[*d*]imidazol-5-yl]-1,3,4-oxadiazol-2-ylthio}-*N*-{4-[(*E*)-3-(4-methoxyphenyl)acryloyl]phenyl}acetamide (7h) Beige crystal (0.19 g, 82% yield); m.p: 228–230 °C; ^{1} H NMR (400 MHz, DMSO-d_6) δ (ppm): 3.81 (3 H, s, OCH3), 4.26 (0.60 H, s, SCH2), 4.46 (1.40 H, s, SCH2), 7.01 (2 H, d, *J*=8.8 Hz, Ar-H), 7.22–7.24 (2 H, m, 1 Ar-H+CH=CH), 7.60–7.66 (2 H, m, Ar-H), 7.69 (1 H, d, *J*=15.5 Hz, CH=CH), 7.78–7.84 (4 H, m, Ar-H), 8.12–8.17 (4 H, m, Ar-H), 8.37–8.41 (2 H, m, Ar-H), 11.00 (1 H, s, NH); ^{13} C NMR (125 MHz, DMSO-d_6) δ (ppm): 45.51, 55.42, 113.69, 114.44, 118.66, 119.46, 122.53, 122.59, 123.68, 127.03, 127.12, 127.27, 127.42, 129.89, 130.76, 133.02, 133.15, 142.90, 143.54, 149.98, 161.33, 163.66, 164.84, 164.92, 165.68, 168.97, 187.53; Anal. calcd. for $C_{33}H_{24}ClN_5O_4S$: C 63.71, H 3.89, N 11.26, S 5.15. Found: C 63.98, H 4.05, N 11.51, S 5.23.

2-{5-[2-(4-Chlorophenyl)-1 *H*-benzo[*d*]imidazol-5-yl]-1,3,4-oxadiazol-2-ylthio}-*N*-{4-[(*E*)-3-(3,4-dimethoxyphenyl)acryloyl]phenyl}acetamide (7i) Pale brown powder (0.23 g, 83% yield); m.p: 208–210 °C; ^{1} H NMR (400 MHz, DMSO-d_6) δ (ppm): 3.81 (3 H, s, OCH3), 3.86 (3 H, s, OCH3), 4.45 (2 H, s, SCH2), 7.01 (1 H, d, *J*=8.3 Hz, Ar-H), 7.25 (1 H, d, *J*=8.3 Hz, Ar-H), 7.36 (1 H, d, *J*=8.3 Hz, Ar-H), 7.52 (1 H, s, Ar-H), 7.72–7.78 (2 H, m, 1 Ar-H+CH=CH), 7.80–7.84 (4 H, m, 3 Ar-H+CH=CH), 8.13 (2 H, d, *J*=8.5 Hz, Ar-H), 8.18 (2 H, d, *J*=8.5 Hz, Ar-H), 8.36 (2 H, d, *J*=8.3 Hz, Ar-H), 10.96 (1 H, s, NH), 13.48 (1 H, s, NH); ^{13} C NMR (125 MHz, DMSO-d_6) δ (ppm): 46.02, 56.08, 56.25, 111.25, 112.06, 113.58, 119.08, 119.99, 124.31, 124.36, 124.43, 124.47, 127.47, 127.78, 127.85, 128.08, 130.27, 130.33, 133.08, 133.12, 133.50, 143.31, 144.42, 144.47, 149.52, 151.71, 164.14, 165.30, 166.07, 187.95; Anal. calcd. for $C_{34}H_{26}ClN_5O_5S$: C 62.62, H 4.02, N 10.74, S 4.92. Found: C 62.84, H 4.19, N 11.03, S 5.01.

2-{5-[2-(4-Chlorophenyl)-1 *H*-benzo[*d*]imidazol-5-yl]-1,3,4-oxadiazol-2-ylthio}-*N*-{4-[(*E*)-3-(3,4,5-trimethoxyphenyl)acryloyl]phenyl}acetamide (7j) Beige powder (0.20 g, 82% yield); m.p: 223–225 °C; ^{1} H NMR (400 MHz, DMSO-d_6) δ (ppm): 3.71 (3 H, s, OCH3), 3.86 (6 H, s, OCH3), 4.32 (0.40 H, s, SCH2), 4.45 (1.60 H, s, SCH2), 7.16–7.28 (4 H, m, Ar-H), 7.56–7.62 (1 H, m, Ar-H), 7.67 (1 H, d, *J*=15.5 Hz, CH=CH), 7.81 (2 H, d, *J*=8.8 Hz, Ar-H), 7.89 (1 H, d, *J*=15.5 Hz, CH=CH), 8.14 (2 H, d, *J*=8.4 Hz, Ar-H), 8.19 (2 H, d, *J*=8.8 Hz, Ar-H), 8.35 (2 H, d, *J*=8.4 Hz, Ar-H), 10.89 (1 H, s, NH), 13.39 (1 H, s, NH); ^{13} C NMR (125 MHz, DMSO-d_6) δ (ppm): 46.18, 56.63, 60.62, 107.00, 113.44, 119.09, 121.60, 122.96, 124.46, 126.91, 127.49, 127.78, 127.85, 130.42, 130.46, 130.77, 133.11, 133.33, 140.22, 143.41, 143.47, 144.48, 153.59, 164.16, 165.31, 166.08, 166.32, 188.02; Anal. calcd. for $C_{35}H_{28}ClN_5O_6S$: C 61.63, H 4.14, N 10.27, S 4.70. Found: C 61.83, H 4.32, N 10.53, S 4.83.

2-{5-[2-(4-Methoxyphenyl)-1 *H*-benzo[*d*]imidazol-5-yl]-1,3,4-oxadiazol-2-ylthio}-*N*-{4-[(*E*)-3-phenylacryloyl]phenyl}acetamide (7k) Orange crystal (0.11 g, 74% yield); m.p: 178–180 °C; ^{1} H NMR (500 MHz, DMSO-d_6) δ (ppm): 3.86 (3 H, s, OCH3), 4.34 (2 H, s, SCH2), 7.14 (2 H, d, *J*=8.3 Hz, Ar-H), 7.37–7.46 (5 H, m, Ar-H), 7.73 (1 H, d, *J*=15.4 Hz, CH=CH), 7.78 (2 H, d, *J*=8.3 Hz, Ar-H), 7.83–7.89 (3 H, m, Ar-H), 7.95 (1 H, d, *J*=15.4 Hz, CH=CH), 8.15–8.21 (4 H, m, Ar-H), 10.79 (1 H, s, NH), 13.10 (1 H, s, NH); ^{13} C NMR (125 MHz, DMSO-d_6) δ (ppm): 46.12, 55.85, 114.93, 114.95, 119.05, 119.09, 121.71, 122.42, 128.73, 128.76, 128.84, 129.27, 129.33, 129.36, 129.76, 130.44, 130.48, 130.97, 131.00, 133.08, 133.10, 135.22, 143.53, 143.94, 165.32, 166.32, 188.03; HRMS (ESI) m/z $[M+H]^+$ calcd. for $C_{33}H_{25}N_5O_4S$: 588.1700, found: 588.1643.

2-{5-[2-(4-Methoxyphenyl)-1 *H*-benzo[*d*]imidazol-5-yl]-1,3,4-oxadiazol-2-ylthio}-*N*-{4-[(*E*)-3-(4-chlorophenyl)acryloyl]phenyl}acetamide (7l) Pale brown crystal (0.23 g, 80% yield); m.p: 245–247 °C; ^{1} H NMR (500 MHz, DMSO-d_6) δ (ppm): 3.89 (3 H, s, OCH3), 4.26 (1 H, s, SCH2), 4.35 (1 H, s, SCH2), 7.17–7.24 (2 H, m, Ar-H), 7.51 (2 H, d, *J*=8.2 Hz, Ar-H), 7.70 (1 H, d, *J*=15.6 Hz, CH=CH), 7.76–7.81 (2 H, m, 1

Ar-H+CH=CH), 7.83 (1 H, d, *J*=8.2 Hz, Ar-H), 7.92 (2 H, d, *J*=8.4 Hz, Ar-H), 7.98 (1 H, d, *J*=8.4 Hz, Ar-H), 8.15–8.19 (3 H, m, Ar-H), 8.28 (2 H, m, Ar-H), 8.34 (1 H, d, *J*=8.4 Hz, Ar-H), 10.98 (1 H, s, NH); ^{13} C NMR (125 MHz, DMSO-d_6) δ (ppm): 45.86, 55.86, 114.37, 115.00, 115.52, 119.04, 119.26, 123.14, 125.22, 125.76, 126.34, 129.37, 129.81, 130.17, 130.44, 130.48, 130.59, 130.94, 132.98, 134.19, 135.41, 143.12, 143.64, 166.17, 166.46, 167.29, 187.81; Anal. calcd. for $C_{33}H_{24}ClN_5O_4S$: C 63.71, H 3.89, N 11.26, S 5.15. Found: C 63.52, H 4.03, N 11.52, S 5.23.

2-{5-[2-(4-Methoxyphenyl)-1 *H*-benzo[*d*]imidazol-5-yl]-1,3,4-oxadiazol-2-ylthio}-*N*-{4-[(*E*)-3-(4-methoxyphenyl)acryloyl]phenyl}acetamide (7m) Beige Crystal (0.13 g, 81% yield); m.p: 247–249 °C; ^{1} H NMR (500 MHz, DMSO-d_6) δ (ppm): 3.82 (3 H, s, OCH3), 3.85 (H, s, OCH3), 4.25 (1.25 H, s, SCH2), 4.43 (0.75 H, s, SCH2), 6.95–7.03 (2 H, m, Ar-H), 7.12–7.15 (3 H, m, Ar-H), 7.71 (1 H, d, *J*=15.3 Hz, CH=CH), 7.80–7.85 (5 H, m, Ar-H+CH=CH), 8.09–8.20 (6 H, m, Ar-H), 10.90 (1 H, s, NH), 13.32 (1 H, s, NH); ^{13} C NMR (125 MHz, DMSO-d_6) δ (ppm): 46.05, 55.84, 55.85, 114.84, 114.94, 116.83, 116.86, 119.06, 119.86, 120.78, 122.38, 127.85, 128.83, 128.90, 130.30, 131.15, 133.27, 133.43, 143.20, 144.01, 154.06, 154.36, 161.55, 162.94, 166.00, 166.51, 169.50, 187.80; HRMS (ESI) m/z $[M+H]^+$ calcd. for $C_{34}H_{27}N_5O_5S$: 618.1806, found: 618.1737.

2-{5-[2-(4-Methoxyphenyl)-1 *H*-benzo[*d*]imidazol-5-yl]-1,3,4-oxadiazol-2-ylthio}-*N*-{4-[(*E*)-3-(3,4-dimethoxyphenyl)acryloyl]phenyl}acetamide (7n) Pale brown crystal (0.19 g, 78% yield); m.p: 222–224 °C; ^{1} H NMR (500 MHz, DMSO-d_6) δ (ppm): 3.81 (3 H, s, OCH3), 3.87 (6 H, s, 2OCH3), 4.35 (0.87 H, s, SCH2), 4.45 (1.13 H, s, SCH2), 7.00 (1 H, d, *J*=8.6 Hz, Ar-H), 7.18 (1 H, d, *J*=8.4 Hz, Ar-H), 7.23 (1 H, d, *J*=8.4 Hz, Ar-H), 7.36 (1 H, d, *J*=8.6 Hz, Ar-H), 7.53 (1 H, s, Ar-H), 7.67 (1 H, d, *J*=15.6 Hz, CH=CH), 7.69–7.85 (4 H, m, Ar-H+CH=CH), 7.91 (1 H, d, *J*=8.6 Hz, Ar-H), 8.00 (1 H, d, *J*=8.6 Hz, Ar-H), 8.15–8.19 (2 H, m, Ar-H), 8.25 (1 H, s, Ar-H), 8.30 (1 H, d, *J*=8.8 Hz, Ar-H), 11.00 (1 H, s, NH), 13.30 (1 H, s, NH); ^{13} C NMR (125 MHz, DMSO-d_6) δ (ppm): 44.37, 56.05, 56.16, 56.21, 110.97, 112.10, 114.18, 115.29, 115.51, 119.02, 119.32, 119.86, 124.40, 125.73, 127.90, 129.35, 129.81, 130.17, 130.29, 130.32, 133.56, 142.97, 144.31, 149.37, 151.24, 151.76, 152.90, 162.28, 163.10, 167.65, 187.50; Anal. calcd. for $C_{35}H_{29}N_5O_6S$: C 64.90, H 4.51, N 10.81, S 4.95. Found: C 65.07, H 4.69, N 11.05, S 5.01.

2-{5-[2-(4-Methoxyphenyl)-1 *H*-benzo[*d*]imidazol-5-yl]-1,3,4-oxadiazol-2-ylthio}-*N*-{4-[(*E*)-3-(3,4,5-trimethoxyphenyl)acryloyl]phenyl}acetamide (7o) Pale brown Crystal (0.21 g, 86% yield); m.p: 154–156 °C; ^{1} H NMR (500 MHz, DMSO-d_6) δ (ppm): 3.71 (3 H, s, OCH3), 3.84 (3 H, s, OCH3), 3.86 (6 H, s, 2OCH3), 4.39 (0.30 H, s, SCH2), 4.46 (1.70 H, s, SCH2), 7.15 (2 H, d, *J*=8.8 Hz, Ar-H), 7.23 (2 H, s, Ar-H), 7.67 (1 H, d, *J*=8.0 Hz, Ar-H), 7.71 (1 H, d, *J*=15.5 Hz, CH=CH), 7.86 (2 H, d, *J*=8.8 Hz, Ar-H), 7.91 (1 H, d, *J*=15.5 Hz, CH=CH), 8.20 (3 H, d, *J*=8.5 Hz, Ar-H), 8.25 (3 H, d, *J*=8.5 Hz, Ar-H), 11.16 (1 H, s, NH), 13.38 (1 H, s, NH); ^{13} C NMR (125 MHz, DMSO-d_6) δ (ppm): 44.32, 55.94, 56.63, 57.81, 106.96, 114.81, 114.96, 114.99, 115.02, 116.87, 119.03, 119.06, 121.72, 129.15, 129.22, 129.25, 130.43, 130.74, 132.98, 140.00, 140.15, 143.48, 144.31, 153.52, 153.55, 161.76, 166.02, 168.18, 188.00; HRMS (ESI) m/z $[M+H]^+$ calcd. for $C_{36}H_{31}N_5O_7S$: 678.2017, found: 678.2090.

2-{5-[2-(3,4-Dimethoxyphenyl)-1 *H*-benzo[*d*]imidazol-5-yl]-1,3,4-oxadiazol-2-ylthio}-*N*-{4-[(*E*)-3-phenylacryloyl]phenyl}acetamide (7p) Orange powder (0.18 g, 89.32% yield); m.p: 185–186 °C; ^{1} H NMR (500 MHz, DMSO-d_6) δ (ppm): 3.85 (3 H, s, OCH3), 3.90 (3 H, s, OCH3), 4.26 (0.60 H, s, SCH2), 4.43 (1.40 H, s, SCH2), 7.16 (1 H, s, Ar-H), 7.40–7.55 (3 H, m, Ar-H), 7.65 (1 H, s, Ar-H), 7.74 (1 H, d, *J*=15.4 Hz, CH=CH), 7.77–7.83 (5 H, m, Ar-H), 7.88–7.97 (3 H, m, 2 Ar-H+CH=CH), 8.08–8.20 (2 H, m, Ar-H), 8.26–8.28 (1 H, m, Ar-H), 10.88 (1 H, s, NH), 13.31(1 H, s, NH); ^{13} C NMR (125 MHz, DMSO-d_6) δ (ppm): 46.01, 56.10, 56.23, 110.41, 112.31, 112.32, 116.86, 117.16, 119.09, 120.16, 122.22, 122.36, 129.27, 129.32, 129.36, 129.40, 129.77, 130.48, 131.10, 131.40, 133.27, 135.13, 137.82, 143.49, 143.95, 149.41, 151.29, 163.10, 166.29, 188.03; HRMS (ESI) m/z $[M+H]^+$ calcd. for $C_{34}H_{27}N_5O_5S$: 618.1806, found: 618.1865.

2-{5-[2-(3,4-Dimethoxyphenyl)-1 *H*-benzo[*d*]imidazol-5-yl]-1,3,4-oxadiazol-2-ylthio}-*N*-{4-[(*E*)-3-(4-chlorophenyl)acryloyl]phenyl}acetamide (7q) Brown powder (0.12 g, 84.62% yield); m.p: 194–195 °C; ^{1} H NMR (500 MHz, DMSO-d_6) δ (ppm): 3.85 (3 H, s, OCH3), 3.91 (3 H, s, OCH3), 4.14 (1.20 H, s, SCH2), 4.36 (0.80 H, s, SCH2), 7.15 (1 H, d, *J*=6.6 Hz, Ar-H), 7.52 (2 H, d, *J*=8.8 Hz, Ar-H), 7.71 (1 H, d, *J*=15.2 Hz, CH=CH), 7.75 (1 H, s, Ar-H), 7.80 (2 H, d, *J*=8.0 Hz, Ar-H), 7.84 (3 H, d, *J*=8.8 Hz, Ar-H), 7.92 (2 H, d, *J*=8.0 Hz, Ar-H), 7.97 (1 H, d, *J*=15.2 Hz, CH=CH)), 8.12 (1 H, s, Ar-H), 8.15–8.22 (2 H, d, *J*=8.8 Hz, Ar-H), 10.98 (1 H, s, NH), 13.28 (1 H, s, NH); ^{13} C NMR (125 MHz, DMSO-d_6) δ (ppm): 45.80, 56.10, 56.15, 110.49, 112.29, 116.98, 119.01, 119.10, 120.34, 120.36, 122.49, 123.16, 129.31, 129.38, 130.45, 130.49, 130.96, 132.95, 133.01, 134.20, 134.59, 135.42, 142.42, 143.63, 143.66, 149.39, 151.24, 162.00, 166.53, 187.79; HRMS (ESI) m/z $[M+H]^+$ calcd. for $C_{34}H_{26}ClN_5O_5S$: 652.1416, found: 652.1367.

2-{5-[2-(3,4-Dimethoxyphenyl)-1 *H*-benzo[*d*]imidazol-5-yl]-1,3,4-oxadiazol-2-ylthio}-*N*-{4-[(*E*)-3-(4-methoxyphenyl)acryloyl]phenyl}acetamide (7r) Beige powder (0.15 g, 78.62% yield); m.p: 170–171 °C; ^{1} H NMR (500 MHz, DMSO-d_6) δ (ppm): 3.83 (3 H, s, OCH_3), 3.86 (3 H, s, OCH3), 3.90 (3 H, s, OCH3), 4.34 (1.60 H, s, SCH2), 4.43 (0.40 H, s, SCH2), 7.02 (2 H, d, *J*=8.5 Hz, Ar-H), 7.16 (1 H, d, *J*=8.5 Hz, Ar-H), 7.64 (1 H, s, Ar-H), 7.70 (1 H, d, *J*=15.6 Hz, CH=CH), 7.76–7.84 (7 H, m, Ar-H+CH=CH), 7.86 (1 H, s, Ar-H), 8.13–8.20 (3 H, m, Ar-H), 10.83 (1 H, s, NH), 13.29 (1 H, s, NH); ^{13} C NMR (125 MHz, DMSO-d_6) δ (ppm): 45.98, 55.84, 56.11, 56.12, 110.43, 110.44, 112.31, 114.86, 115.52, 116.88, 118.89, 119.02, 119.03, 119.86, 119.89, 120.18, 120.21, 122.59, 124.69, 124.72, 124.89, 125.04, 127.86, 130.27, 131.16, 143.70, 149.39, 151.02, 161.75, 168.17, 187.79; Anal. calcd. for $C_{35}H_{29}N_5O_6S$: C 64.90, H 4.51, N 10.81, S 4.95. Found: C 64.79, H 4.63, N 11.02, S 4.92.

2-{5-[2-(3,4-Dimethoxyphenyl)-1 *H*-benzo[*d*]imidazol-5-yl]-1,3,4-oxadiazol-2-ylthio}-*N*-{4-[(*E*)-3-(3,4-dimethoxyphenyl)acryloyl]phenyl}acetamide (7s) Brown powder (0.20 g, 86.30% yield); m.p: 190–193 °C; ^{1} H NMR (500 MHz, DMSO-d_6) δ (ppm): 3.82 (3 H, s, OCH3), 3.85 (3 H, s, OCH3), 3.87 (3 H, s, OCH3), 3.90 (3 H, s, OCH3), 4.26 (0.50 H, s, SCH2), 4.43 (1.50 H, s, SCH2), 6.98–7.07 (1 H, m, Ar-H), 7.15 (1 H, d, *J*=8.2 Hz, Ar-H), 7.37–7.44 (2 H, m, Ar-H), 7.56 (1 H, d, *J*=15.6 Hz, CH=CH), 7.62–7.69 (1 H, m, Ar-H), 7.71 (1 H, s, Ar-H), 7.82 (4 H, d, *J*=8.8 Hz, Ar-H), 7.87 (1 H, d, *J*=15.6 Hz, CH=CH), 8.13 (1 H, s, Ar-H), 8.20 (1 H, d, *J*=8.8 Hz, Ar-H), 8.31 (1 H, d, *J*=8.8 Hz, Ar-H), 10.88 (1 H, s, NH), 13.32 (1 H, s, NH); ^{13} C NMR (125 MHz, DMSO-d_6) δ (ppm): 46.02, 56.05, 56.10, 56.21, 110.35, 110.41, 111.01, 112.00, 112.05, 112.30, 112.35, 116.87, 118.59, 118.95, 119.04, 119.88, 119.92, 122.39, 124.34, 128.06, 130.32, 130.35, 144.52, 149.41, 149.47, 151.13, 151.30, 151.65, 151.90, 165.74, 166.18, 166.62, 188.01; HRMS (ESI) m/z $[M+H]^+$ calcd. for $C_{36}H_{31}N_5O_7S$: 678.2017, found 678.1952.

2-{5-[2-(3,4-Dimethoxyphenyl)-1 *H*-benzo[*d*]imidazol-5-yl]-1,3,4-oxadiazol-2-ylthio}-*N*-{4-[(*E*)-3-(3,4,5-trimethoxyphenyl)acryloyl]phenyl}acetamide (7t) Brown crystal (0.165 g, 79.35% yield); m.p: 190–193 °C; ^{1} H NMR (500 MHz, DMSO-d_6) δ (ppm): 3.72 (3 H, s, OCH3), 3.85 (3 H, s, OCH3), 3.87 (6 H, s, 2OCH3), 3.90 (3 H, s, OCH3), 4.24 (0.75 H, s, SCH2), 4.43 (1.25 H, s, SCH2), 7.14–7.17 (1 H, m, Ar-H), 7.23 (2 H, s, Ar-H), 7.26 (1 H, d, *J*=8.6 Hz, Ar-H)), 7.65–7.70 (2 H, m, 1 Ar-H+CH=CH), 7.78 (1 H, s, Ar-H), 7.81 (3 H, d, *J*=8.6 Hz, Ar-H), 7.84 (1 H, s, Ar-H), 7.90 (1 H, d, *J*=15.4 Hz, CH=CH), 8.21 (1 H, d, *J*=8.4 Hz, Ar-H), 8.31 (1 H, d, *J*=8.4 Hz, Ar-H), 10.91 (1 H, s, NH), 13.24 (1 H, s, NH); ^{13} C NMR (125 MHz, DMSO-d_6) δ (ppm): 46.05, 56.10, 56.59, 56.65, 60.60, 107.24, 110.15, 112.31, 116.65, 118.80, 121.20, 121.50, 127.89, 128.43, 129.77, 130.59, 131.12, 133.25, 139.46, 139.98, 140.29, 143.19, 143.49, 145.35, 145.65, 146.69, 149.08, 153.72, 159.07, 164.44, 166.54, 189.12; HRMS (ESI) m/z $[M+H]^+$ calcd. for $C_{37}H_{33}N_5O_8S$: 708.2123, found 708.2062.

2-{5-[2-(3,4,5-Trimethoxyphenyl)-1 *H*-benzo[*d*]imidazol-5-yl]-1,3,4-oxadiazol-2-ylthio}-*N*-{4-[(*E*)-3-phenylacryloyl]phenyl}acetamide (7u) Brown crystal (0.13 g, 73.35% yield); m.p: 188–190 °C; ^{1} H NMR (500 MHz, DMSO-d_6) δ (ppm): 3.92 (6 H, s, 2OCH3), 3.94 (3 H, s, OCH3), 4.36 (1.25 H, s, SCH2), 4.46 (0.75 H, s, SCH2), 7.42–7.46 (4 H, m, Ar-H), 7.71 (2 H, d, *J*=8.6 Hz, Ar-H), 7.75 (1 H, d, *J*=15.6 Hz, CH=CH), 7.80–7.84 (2 H, m, 1 Ar-H+CH=CH), 7.88 (2 H, s, Ar-H), 7.93 (1 H, d, *J*=6.6 Hz, Ar-H), 7.95–8.01 (1 H, m, Ar-H), 8.16 (3 H, d, *J*=8.6 Hz, Ar-H), 10.90 (1 H, s, NH); ^{13} C NMR (125 MHz, DMSO-d_6) δ (ppm): 44.46, 56.68, 57.58, 110.16, 112.69, 114.10, 119.25, 120.67, 122.08, 122.98, 124.11, 124.40, 124.62, 129.77, 130.59, 130.88, 131.18, 132.08, 135.43, 141.41, 143.71, 148.56, 151.11, 153.64, 154.23, 162.72, 165.35, 187.79; Anal. calcd. for $C_{35}H_{29}N_5O_6S$: C 64.90, H 4.51, N 10.81, S 4.95. Found: C 65.12, H 4.68, N 10.97, S 5.03.

2-{5-[2-(3,4,5-Trimethoxyphenyl)-1 *H*-benzo[*d*]imidazol-5-yl]-1,3,4-oxadiazol-2-ylthio}-*N*-{4-[(*E*)-3-(4-chlorophenyl)acryloyl]phenyl}acetamide (7v) Brown crystal (0.16 g, 77.54% yield); m.p: 196–198 °C; ^{1} H NMR (500 MHz, DMSO-d_6) δ (ppm): 3.75 (6 H, s, OCH3), 3.76 (3 H, s, 2OCH3), 4.25 (0.75 H, s, SCH2), 4.43 (1.25 H, s, SCH2), 7.51–7.52 (5 H, m, 4 Ar-H+CH=CH), 7.72 (2 H, d, *J*=6.6 Hz, Ar-H), 7.77–7.82 (2 H, m, 1 Ar-H+CH=CH), 7.94 (2 H, s, Ar-H), 7.97 (2 H, d, *J*=6.6 Hz, Ar-H), 8.15 (1 H, d, *J*=8.5 Hz, Ar-H), 8.20 (1 H, d, *J*=6.6 Hz, Ar-H), 10.92 (1 H, s, NH); ^{13} C NMR (125 MHz, DMSO-d_6) δ (ppm): 46.02, 56.47, 60.78, 117.17, 119.03, 121.50, 123.13, 123.16, 123.19, 128.46, 129.38, 130.06, 130.29, 130.95, 130.97, 131.01, 134.32, 135.41, 135.43, 135.52, 136.48, 142.15, 142.45, 153.72, 153.74, 163.32, 164.66, 188.00; HRMS (ESI) m/z $[M+H]^+$ calcd. for $C_{35}H_{28}ClN_5O_6S$: 682.1522, found: 682.1471.

2-{5-[2-(3,4,5-Trimethoxyphenyl)-1 *H*-benzo[*d*]imidazol-5-yl]-1,3,4-oxadiazol-2-ylthio}-*N*-{4-[(*E*)-3-(4-methoxyphenyl)acryloyl]phenyl}acetamide (7w) Brown crystal (0.163 g, 76.65% yield); m.p: 200–204 °C; ^{1} H NMR (500 MHz, DMSO-d_6) δ (ppm): 3.76 (3 H, s, OCH3), 3.82 (3 H, s, OCH3), 3.93 (6 H, s, 2OCH3), 4.26 (0.70 H, s, SCH2), 4.45 (1.30 H, s, SCH2), 7.00-7.02 (2 H, m, Ar-H), 7.69 (2 H, d, *J*=6.6 Hz, Ar-H), 7.77 (2 H, d, *J*=6.6 Hz, Ar-H), 7.80 (1 H, d, *J*=15.4 Hz,

CH=CH), 7.83 (2 H, d, *J*=6.6 Hz, Ar-H), 7.84–7.87 (3 H, m, Ar-H+CH=CH), 8.15–8.18 (3 H, m, Ar-H), 11.06 (1 H, s, NH); ^{13} C NMR (125 MHz, DMSO-d_6) δ (ppm): 44.23, 55.86, 56.99, 60.41, 105.01, 114.71, 118.65, 119.85, 122.26, 122.67, 127.23, 128.35, 129.47, 130.89, 130.94, 135.90, 142.61, 142.82, 144.03, 148.83, 149.09, 152.50, 153.11, 153.13, 161.62, 162.43, 162.73, 166.16, 187.79; HRMS (ESI) m/z $[M+H]^+$ calcd. for $C_{36}H_{31}N_5O_7S$: 678.2017, found: 678.1996.

2-{5-[2-(3,4,5-Trimethoxyphenyl)-1 *H*-benzo[*d*] imidazol-5-yl]-1,3,4-oxadiazol-2-ylthio}-*N*-{4-[(*E*)-3-(3,4-dimethoxyphenyl)acryloyl]phenyl}acetamide (7x) Brown crystal (0.21 g, 86.50% yield); m.p: 212–215°C; ^{1} H NMR (500 MHz, DMSO-d_6) δ (ppm): 3.82 (3 H, s, OCH3), 3.87 (3 H, s, OCH3), 3.92 (6 H, s, 2OCH3), 3.93 (3 H, s, OCH3), 4.36 (1.25 H, s, SCH2), 4.45 (0.75 H, s, SCH2), 7.02 (1 H, d, *J*=8.8 Hz, Ar-H), 7.36–7.39 (1 H, m, Ar-H), 7.66–7.72 (3 H, m, 2 Ar-H+CH=CH), 7.76–7.79 (2 H, m, 1 Ar-H+CH=CH), 7.81 (2 H, s, Ar-H), 8.83 (2 H, d, *J*=7.5 Hz, Ar-H), 8.15–8.19 (3 H, m, Ar-H), 11.03 (1 H, s, NH); ^{13} C NMR (125 MHz, DMSO-d_6) δ (ppm); 44.46, 54.42, 56.06, 56.22, 56.97, 104.78, 110.45, 111.88, 117.22, 119.16, 119.34, 120.02, 122.57, 124.10, 124.47, 124.63, 128.08, 130.26, 132.90, 133.40, 139.78, 139.97, 144.97, 145.30, 148.64, 149.41, 151.39, 151.59, 160.22, 164.69, 167.57, 187.78; Anal. calcd. for $C_{37}H_{33}N_5O_8S$: C 62.79, H 4.70, N 9.90, S 4.53. Found: C 62.95, H 4.82, N 10.16, S 4.60.

Biology

Screening of anti-proliferative activity by NCI

The methodology of the NCI anti-proliferative screening has been described in details elsewhere (http://www.dtp.nci.nih.gov).

Cytotoxic activity using MTT assay and determination of IC_{50}

Assay for anti-proliferative effect in melanoma LOX-IMVI cell lines Using the propidium iodide fluorescence assay with Staurosporine as the reference drug, the anti-proliferative activities of compounds **7g**, **7l**, **7p**, **7q**, and **7v**, was carried out according to a previously reported procedure[31, 32] to detect IC_{50} against LOX-IMVI cell lines. compounds 7g, 7l, 7p, 7q, and 7v were incubated with LOX-IMVI cells for 2 days. See Appendix A.

Assay for anti-proliferative effect Using the propidium iodide fluorescence assay with doxorubicin as the reference drug, IC_{50} of the 24 compounds **7a-x**, was carried out according to a previously reported procedure[31, 32] against a panel of four human cancer cell lines; epithelial cancer cell line (A-549), breast cancer cell line (MCF-7), colon cancer cell line (HT-29) and pancreas cancer cell line (Panc-1). Compounds **7a-x** were incubated with cancer cells for 2 days at different concentrations. See Appendix A.

Cell viability determination MTT assay was done to determine the effect of the synthesized compounds on the viability of mammary epithelial cells (MCF-10 A) [33, 34]. Compounds **7a-x** were incubated with MCF-10 A cells for 4 days at 50 μM concentration, and the viability of cells was determined. See Appendix A.

EGFR inhibitory assay

The inhibitory efficacy of of the most active compounds **7e**, **7g**, **7h**, **7k-n**, **7p**, **7q**, and **7v** against EGFR was evaluated using the EGFR-TK assay [35, 36]. See Appendix A.

BRAF kinase assay

Compounds **7e**, **7g**, **7h**, **7k-n**, **7p**, **7q**, and **7v** were further examined for their ability to inhibit the V600E mutant BRAF using kinase assay against $BRAF^{V600E}$. [24, 37] See Appendix A.

Apoptosis-induction activity detection

Caspases assays The effect of compounds; **7k**, **7l**, and **7m** on caspases-3,8,9 was determined and compared to doxorubicin as a control according to reported assays [38]. See Appendix A.

Cytochrome C assay Compounds **7k**, **7l**, and **7m** were evaluated as Cytochrome C activators in the MCF-7 human breast cancer cell line according to previously reported assays [39]. See Appendix A.

BAX activation assay The most potent caspase activators **7k**, **7l**, and **7m** were investigated for their influence on BAX level in a breast cancer cell line (MCF-7) using doxorubicin as a control according to reported assay [38]. See Appendix A.

Bcl-2 Inhibition assay The most potent caspase activators **7k**, **7l**, and **7m** were examined for their influence on Bacl-2 level in a breast cancer cell line (MCF-7) using doxorubicin as a control according to reported assay [38]. See Appendix A.

Cell apoptosis assay

Apoptosis was determined by flow cytometry based on the Annexin-V-fluoresce in isothiocyanate (FITC) and propidium iodide (PI) staining kit (BD Pharmingen, San Diego, USA) [40, 41] See Appendix A.

Docking studies

The most bioactive derivatives (i.e. **7e**, **7g**, **7h**, **7k-n**, **7p**, **7q**, and **7v**) were drawn and docked in the active site of EGFR (PDB ID: 1M17) [48–50] and BRAF (PDB

ID: 3OG7) using AutoDock Vina software program as reported in the literature. See Appendix A.

Supplementary Information

The online version contains supplementary material available at https://doi.org/10.1186/s13065-023-01003-3.

Supplementary Material 1

Supplementary Material 2

Acknowledgements

The authors thank the Development Therapeutics Program of the **National Cancer Institute**, Bethesda, MD, USA, for in vitro evaluation of the anti-proliferative activity. Grateful thanks are expressed to **Professor Robert Young**, PhD, FCIC, FRSC, MC, Merck Frosst - B.C. Discovery Chair in Pharmaceutical Genomics, Bioinformatics and Drug Discovery, Department of Chemistry, Simon Fraser University, Canada, for helping in measuring the NMR data. The authors also acknowledge the efforts of **Professor Jeffrey Christoff**, PhD, Professor of Medicinal Chemistry, Raabe College of Pharmacy, Ohio Northern University, USA, for proofreading the manuscript.

Authors' contributions

The manuscript was written through contributions of all authors. All authors have given approval to the final version of the manuscript.1- Fatma Hagar First author, carried out all organic synthesis of compounds and analysis of spectrophotometric data. Involved in writing the synthesis experimental details and data in the manuscript.2- Samar Abbas Principal investigator, a committee member involved with the design and execution of organic synthetic procedures and schemes, revised experimental data and principal contributor in writing and revising the manuscript.3- Hesham Gomaa Carried out biological testing. Involved in writing the details of biological and biochemical tests and data in the manuscript.4- Bahaa Youssif Principal investigator, a committee member involved with the design and execution of biological investigations and contributed in revising the manuscript.5- Ahmed Sayed Carried out molecular modelling studies. Involved in writing the details of docking studies in the manuscript.6- Dalia Abdelhamid* Principal investigator, a committee member involved with the design and execution of organic synthetic procedures and schemes and principal contributor in writing and revising the manuscript. Responsible for all journal communications.7- Mohamed Abdel-Aziz Principal investigator, a committee member involved with the design and execution of organic synthetic procedures and schemes and principal coordinator of the whole research project. Involved in revising the manuscript.

Funding

Not applicable.

Data Availability

Data and materials of our Figures or Tables are available with us.

Declarations

Ethics approval and consent to participate

Not applicable because of no human or animal are directly involved in this research and the cell lines which used in this research were commercially obtained.

Consent for publication

Not applicable.

Competing interests

The authors declare no competing interests.

Received: 6 March 2023 / Accepted: 10 July 2023
Published online: 16 September 2023

References

1. Cortes J, Perez-García JM, Llombart-Cussac A, Curigliano G, El Saghir NS, Cardoso F, Barrios CH, Wagle S, Roman J, Harbeck N, Eniu A, Kaufman PA, Tabernero J, García-Estévez L, Schmid P, Arribas J. Enhancing Global Access to Cancer Medicines. CA Cancer J Clin. 2020;70(2):105–24. https://doi.org/10.3322/caac.21597.
2. Sung H, Ferlay J, Siegel RL, Laversanne M, Soerjomataram I, Jemal A, Bray F. Global Cancer Statistics 2020: GLOBOCAN estimates of incidence and Mortality Worldwide for 36 cancers in 185 countries. CA Cancer J Clin. 2021;71(3):209–49. https://doi.org/10.3322/caac.21660.
3. Cao W, Chen H-D, Yu Y-W, Li N, Chen W-Q. Changing Profiles of Cancer Burden Worldwide and in China: a secondary analysis of the Global Cancer Statistics 2020. Chin Med J (Engl). 2021;134(07):783–91. https://doi.org/10.1097/CM9.0000000000001474.
4. Soran A, Ozbas S, Ozcinar B, Isik A, Dogan L, Senol K, Dag A, Karanlik H, Aytac O, Karadeniz Cakmak G, Dalci K, Dogan M, Sezer YA, Gokgoz S, Ozyar E, Sezgin E, Breast Health Working Group International. Intervention for hepatic and pulmonary metastases in breast Cancer patients: Prospective, multi-institutional Registry Study–IMET, Protocol MF 14 – 02. Ann Surg Oncol. 2022;29(10):6327–36. https://doi.org/10.1245/s10434-022-12239-z.
5. Wilkinson L, Gathani T. Understanding breast Cancer as a Global Health concern. Br J Radiol. 2022;95(1130):20211033. https://doi.org/10.1259/bjr.20211033.
6. Apoptosis. : *A Review of Programmed Cell Death - Susan Elmore*, 2007. https://journals.sagepub.com/doi/full/10.1080/01926230701320337 (accessed 2022-09-13).
7. Carneiro BA, El-Deiry WS. Targeting apoptosis in Cancer Therapy. Nat Rev Clin Oncol. 2020;17(7):395–417. https://doi.org/10.1038/s41571-020-0341-y.
8. *Mitochondrial pathway–mediated apoptosis is associated with erlotinib–induced cytotoxicity in hepatic cells*. https://www.spandidos-publications.com/ol/15/1/783 (accessed 2022-06-03).
9. McArthur K, Kile BT. Apoptotic caspases: multiple or mistaken identities? Trends Cell Biol. 2018;28(6):475–93. https://doi.org/10.1016/j.tcb.2018.02.003.
10. Wang G, Liang E, Ming P, Rui L, Tang C, Lv J, Ge Y, Zhang F, Wang L, Shang J, Yang D, Zhai Y. Antitumor activity of dual BCL-2/BCL-Xl inhibitor Pelcitoclax (APG-1252) in natural Killer/T-Cell lymphoma (NK/TCL). Blood. 2021;138:2062. https://doi.org/10.1182/blood-2021-152207.
11. Green DR. The mitochondrial pathway of apoptosis part II: the BCL-2 protein family. Cold Spring Harb Perspect Biol. 2022;14(6):a041046. https://doi.org/10.1101/cshperspect.a041046.
12. Meliala ITS, Hosea R, Kasim V, Wu S. The Biological Implications of Yin Yang 1 in the Hallmarks of Cancer. Theranostics. 2020;10(9):4183–200. https://doi.org/10.7150/thno.43481.
13. Pfeffer CM, Singh ATK, Apoptosis. A target for Anticancer Therapy. Int J Mol Sci. 2018;19(2):448. https://doi.org/10.3390/ijms19020448.
14. Naik MJ. Mapk Signalling Pathway: role in Cancer Pathogenesis. J Crit Rev. 2019;6(3):1–6.
15. Janecka-Widła A, Majchrzyk K, Mucha-Małecka A, Biesaga B. EGFR/PI3K/Akt/MTOR pathway in Head and Neck squamous cell carcinoma patients with different HPV status. Pol J Pathol. 2022;72(4):296–314. https://doi.org/10.5114/pjp.2021.113073.
16. Gao F, Li M, Liu W, Li W. Inhibition of EGFR Signaling and activation of mitochondrial apoptosis contribute to Tanshinone IIA-Mediated tumor suppression in Non-Small Cell Lung Cancer cells. OncoTargets Ther. 2020;13:2757–69. https://doi.org/10.2147/OTT.S246606.
17. Thomas R, Weihua Z. Rethink of EGFR in Cancer with its kinase independent function on Board. Front Oncol. 2019;9:800.
18. Sun Y, Ai X, Lu S. Tagrisso Incremental Therapy in a case of meningeal metastasis of Lung Cancer with EGFR Mutation: a Case Report. Transl Lung Cancer Res. 2022;11(2):323–30. https://doi.org/10.21037/tlcr-21-451.
19. Das D, Hong J. Recent advancements of 4-Aminoquinazoline derivatives as kinase inhibitors and their applications in Medicinal Chemistry. Eur J Med Chem. 2019;170:55–72. https://doi.org/10.1016/j.ejmech.2019.03.004.
20. Abdelgalil AA, Al-Kahtani HM, Al-Jenoobi FI. Chapter Four - Erlotinib. In *Profiles of Drug Substances, Excipients and Related Methodology*; Brittain, H. G., Ed.; Profiles of Drug Substances, Excipients, and Related Methodology; Academic Press, 2020; Vol. 45, pp 93–117. https://doi.org/10.1016/bs.podrm.2019.10.004.
21. Sigismund S, Avanzato D, Lanzetti L. Emerging functions of the EGFR in Cancer. Mol Oncol. 2018;12(1):3–20. https://doi.org/10.1002/1878-0261.12155.
22. Wu Z, Huang M, Gong Y, Lin C, Guo WBRAF. EGFR inhibitors synergize to increase cytotoxic Effects and decrease stem cell capacities in

BRAF(^{V600E})-Mutant colorectal Cancer cells. Acta Biochim Biophys Sin. 2018;50(4):355–61. https://doi.org/10.1093/abbs/gmy018.
23. Hagar FF, Abbas SH, Abdelhamid D, Gomaa HAM, Youssif BGM, Abdel-Aziz M. New 1,3,4-Oxadiazole-Chalcone/Benzimidazole hybrids as potent Antiproliferative Agents. Arch Pharm. 2023;356(2):2200357. https://doi.org/10.1002/ardp.202200357.
24. Mohassab AM, Hassan HA, Abdelhamid D, Gouda AM, Youssif BGM, Tateishi H, Fujita M, Otsuka M, Abdel-Aziz M. Design and synthesis of Novel Quinoline/Chalcone/1,2,4-Triazole hybrids as potent Antiproliferative Agent Targeting EGFR and BRAFV600E Kinases. Bioorg Chem. 2021;106:104510. https://doi.org/10.1016/j.bioorg.2020.104510.
25. Fathi MAA, Abd El-Hafeez AA, Abdelhamid D, Abbas SH, Montano MM, Abdel-Aziz M. 1,3,4-Oxadiazole/Chalcone hybrids: design, synthesis, and inhibition of Leukemia Cell Growth and EGFR, src, IL-6 and STAT3 activities. Bioorg Chem. 2019;84:150–63. https://doi.org/10.1016/j.bioorg.2018.11.032.
26. Alzahrani HA, Alam MM, Elhenawy AA, Malebari AM, Nazreen S, Synthesis. Antiproliferative, docking and DFT studies of benzimidazole derivatives as EGFR inhibitors. J Mol Struct. 2022;1253:132265. https://doi.org/10.1016/j.molstruc.2021.132265.
27. Ali IH, Abdel-Mohsen HT, Mounier MM, Abo-elfadl MT, El Kerdawy AM, Ghannam IAY, Design. Synthesis and anticancer activity of Novel 2-Arylbenzimidazole/2-Thiopyrimidines and 2-Thioquinazolin-4(3H)-Ones Conjugates as targeted RAF and VEGFR-2 kinases inhibitors. Bioorg Chem. 2022;126:105883. https://doi.org/10.1016/j.bioorg.2022.105883.
28. Jiang Y, Jia S, Li X, Sun Y, Li W, Zhang W, Xu G. An efficient NaHSO 3-Promoted protocol for Chemoselective synthesis of 2-Substituted Benzimidazoles in Water. Chem Pap. 2018;72(5):1265–76.
29. Hagar FF, Abbas SH, Sayed A, Abdelhamid D, Abdel-Aziz M. New Oxadiazole/ Benzimidazole Hybrids: design, synthesis, and Molecular Docking Studies. J Adv Biomed & Pharm Sci. 2023;6:97–106. https://doi.org/10.21608/jabps.2023.190430.1179.
30. Ahmed FF, Abd El-Hafeez AA, Abbas SH, Abdelhamid D, Abdel-Aziz M. New 1,2,4-Triazole-chalcone hybrids induce Caspase-3 dependent apoptosis in A549 Human Lung Adenocarcinoma cells. Eur J Med Chem. 2018;151:705–22. https://doi.org/10.1016/j.ejmech.2018.03.073.
31. Al-Wahaibi LH, Gouda AM, Abou-Ghadir OF, Salem OIA, Ali AT, Farghaly HS, Abdelrahman MH, Trembleau L, Abdu-Allah HHM, Youssif BGM. Design and synthesis of Novel 2,3-Dihydropyrazino[1,2-a]Indole-1,4-Dione derivatives as antiproliferative EGFR and BRAFV600E dual inhibitors. Bioorg Chem. 2020;104:104260. https://doi.org/10.1016/j.bioorg.2020.104260.
32. Gomaa HAM, Shaker ME, Alzarea SI, Hendawy OM, Mohamed FAM, Gouda AM, Ali AT, Morcoss MM, Abdelrahman MH, Trembleau L, Youssif BGM. Optimization and SAR Investigation of Novel 2,3-Dihydropyrazino[1,2-a]Indole-1,4-Dione derivatives as EGFR and BRAFV600E Dual inhibitors with potent antiproliferative and antioxidant activities. Bioorg Chem. 2022;120:105616. https://doi.org/10.1016/j.bioorg.2022.105616.
33. Youssif BG, Mohamed AM, Osman EEA, Abou-Ghadir OF, Elnaggar DH, Abdelrahman MH, Treamblu L, Gomaa HA. 5-Chlorobenzofuran-2-Carboxamides: from allosteric CB1 modulators to potential apoptotic Antitumor Agents. Eur J Med Chem. 2019;177:1–11.
34. Tantawy AH, Meng X-G, Marzouk AA, Fouad A, Abdelazeem AH, Youssif BG, Jiang H, Wang M-Q. Structure-based design, synthesis, and Biological evaluation of Novel Piperine–Resveratrol Hybrids as Antiproliferative Agents Targeting SIRT-2. RSC Adv. 2021;11(41):25738–51.
35. Mohamed FAM, Gomaa HAM, Hendawy OM, Ali AT, Farghaly HS, Gouda AM, Abdelazeem AH, Abdelrahman MH, Trembleau L, Youssif BGM, Design. Synthesis, and Biological evaluation of novel EGFR inhibitors containing 5-Chloro-3-Hydroxymethyl-Indole-2-Carboxamide Scaffold with apoptotic antiproliferative activity. Bioorg Chem. 2021;112:104960. https://doi.org/10.1016/j.bioorg.2021.104960.
36. Elbastawesy MAI, Aly AA, Ramadan M, Elshaier YAMM, Youssif BGM, Brown AB, El-Din A, Abuo-Rahma G. Novel Pyrazoloquinolin-2-Ones: design, synthesis, Docking Studies, and Biological evaluation as antiproliferative EGFR-TK inhibitors. Bioorg Chem. 2019;90:103045. https://doi.org/10.1016/j.bioorg.2019.103045.
37. Youssif BGM, Gouda AM, Moustafa AH, Abdelhamid AA, Gomaa HAM, Kamal I, Marzouk AA. Design and synthesis of New Triarylimidazole derivatives as dual inhibitors of BRAFV600E/P38α with potential antiproliferative activity. J Mol Struct. 2022;1253:132218. https://doi.org/10.1016/j.molstruc.2021.132218.
38. El-Sheref E, Elbastawesy M, Brown A, Shawky A, Gomaa H, Brase S, Youssif B. Design and synthesis of (2-oxo-1,2-Dihydroquinolin-4-yl)-1,2,3-triazole derivatives via click reaction: potential apoptotic antiproliferative agents. Molecules. 2021;26:6798.
39. Santucci R, Sinibaldi F, Cozza P, Polticelli F, Fiorucci L. Cytochrome c: an Extreme Multifunctional protein with a key role in cell fate. Int J Biol Macromol. 2019;136:1237–46. https://doi.org/10.1016/j.ijbiomac.2019.06.180.
40. Abdelbaset MS, Abdel-Aziz M, Abuo-Rahma GE-DA, Abdelrahman MH, Ramadan M, Youssif BGM. Novel quinoline derivatives carrying Nitrones/Oximes nitric oxide donors: design, synthesis, antiproliferative and Caspase-3 activation activities. Arch Pharm (Weinheim). 2019;352(1):1800270. https://doi.org/10.1002/ardp.201800270.
41. Mahmoud MA, Mohammed AF, Salem OIA, Gomaa HAM, Youssif BGM. New 1,3,4-Oxadiazoles linked with the 1,2,3-Triazole Moiety as Antiproliferative Agents Targeting the EGFR tyrosine kinase. Arch Pharm (Weinheim). 2022;355(6):2200009. https://doi.org/10.1002/ardp.202200009.
42. Genheden S, Ryde U. The MM/PBSA and MM/GBSA Methods to Estimate ligand-binding affinities. Expert Opin Drug Discov. 2015;10(5):449–61.
43. Wildman SA, Crippen GM. Prediction of Physicochemical Parameters by Atomic Contributions. J Chem Inf Comput Sci. 1999;39(5):868–73.
44. Lovering F, Bikker J, Humblet C. Escape from Flatland: increasing saturation as an Approach to improving clinical success. J Med Chem. 2009;52(21):6752–6.
45. Ritchie TJ, Ertl P, Lewis R. The graphical representation of ADME-Related Molecule Properties for Medicinal Chemists. Drug Discov Today. 2011;16(1–2):65–72.
46. Pires DE, Blundell TL, Ascher DB. PkCSM: Predicting Small-Molecule Pharmacokinetic and Toxicity Properties using graph-based signatures. J Med Chem. 2015;58(9):4066–72.
47. Pratama MRF, Poerwono H, Siswodiharjo SADMET. Properties of Novel 5- *O* -Benzoylpinostrobin derivatives. J Basic Clin Physiol Pharmacol. 2019;30(6):20190251. https://doi.org/10.1515/jbcpp-2019-0251.
48. Dallakyan S, Olson AJ. Small-Molecule Library Screening by Docking with PyRx. In *Chemical Biology: Methods and Protocols*; Hempel, J. E., Williams, C. H., Hong, C. C., Eds.; Methods in Molecular Biology; Springer: New York, NY, 2015; pp 243–250. https://doi.org/10.1007/978-1-4939-2269-7_19.
49. Seeliger D, de Groot BL. Ligand docking and binding site analysis with PyMOL and Autodock/Vina. J Comput Aided Mol Des. 2010;24(5):417–22. https://doi.org/10.1007/s10822-010-9352-6.
50. Stamos J, Sliwkowski MX, Eigenbrot C. Structure of the epidermal growth factor receptor kinase domain alone and in Complex with a 4-Anilinoquinazoline inhibitor. J Biol Chem. 2002;277(48):46265–72. https://doi.org/10.1074/jbc.M207135200.

Publisher's Note